A 250m annual alpine grassland AGB dataset over the Qinghai-Tibetan Plateau (2000-2019) in China based on in-situ measurements, UAV images, and MODIS Data

Huifang Zhang [1,2,3], Zhonggang Tang[2], Binyao Wang [2], Hongcheng Kan [2] ,Yi Sun[1,2], Yu Qin[3], Baoping Meng[1,2], Meng Li[1,2], Jianjun Chen[4], Yanyan Lv[1,2], Jianguo Zhang[1,2] Shuli Niu[5], Shuhua Yi [1,2,*]

[1]Institute of Fragile Eco-environment, Nantong University, 999 Tongjing Road, Nantong, Jiangsu, 226007, China
[2]School of Geographic Science, Nantong University, 999 Tongjing Road, Nantong, Jiangsu, 226007, China
[3]State Key Laboratory of Cryospheric Sciences, Northwest Institute of Eco-Environment and Resources, Chinese Academy of Sciences, 320 Donggang West Road, Lanzhou 730000, China
[4]College of Geomatics and Geoinformation, Guilin University of Technology, 12 Jiangan Road, Guilin 541004, China;
[5]Key Laboratory of Ecosystem Network Observation and Modeling, Institute of Geographic Sciences and Natural Resources Research, Chinese Academy of Sciences, Beijing, China

Correspondence to: Shuhua Yi (yis@ntu.edu.cn)

Abstract. The alpine grassland ecosystem accounts for 53% of the Qinghai-Tibet Plateau (QTP) area~~, which~~ and is an important ecological protection barrier, but it is fragile and ~~highly~~ vulnerable to climate change. Therefore, continuous monitoring of grassland~~of the~~ aboveground biomass (AGB) ~~of grassland~~ is necessary. Although many studies have mapped the spatial distribution of AGB ~~over~~ for ~~the~~ QTP, the results vary widely due to the limited ground samples and mismatch~~es~~ with satellite pixel scales. This paper proposed a new algorithm using unmanned aerial vehicles (UAVs) as a bridge to re-estimate the grassland AGB ~~over~~ on the QTP from 2000 to 2019. The innovations were as follows: 1) In terms of ~~In the aspect of~~ ground data ~~collection~~acquisition, the spatial scale matching ~~among~~ ~~between~~among the traditional ground~~-~~samples~~quadrat sampling~~, UAV photos, and MODIS pixels was ~~fully~~ considered. ~~From 2015 to 2019~~During 2015-2019, 906 pairs of quadrat-scale ground-UAV sample data ~~at the quadrat scale~~ and 2,602 sets of MODIS pixel-scale UAV data~~-matching the MODIS pixel scale~~ were collected (over 37,000 UAV photos). Therefore, the ground validation samples ~~was~~ were sufficient and ~~scale~~ scale-matched. 2) In terms of model construction, the traditional quadrat scale ($0.25m^2$) was successfully upscaled to the MODIS pixel scale (6,2500 m^2) based on the random forest ~~method~~ and stepwise upscaling ~~scheme~~methods. Compared with previous studies, the scale matching of independent and dependent variables was ~~realized~~achieved, effectively reducing the impact of spatial scale mismatch. The results showed that the correlation between the AGB values estimated by UAV and the MODIS vegetation indices was higher than that of the traditional sampling method at the pixel scale~~At the pixel scale, the AGB value estimated by UAV had a more linear correlation with the MODIS vegetation indices than the traditional sampling method~~. The ~~multi-year independent~~ cross-year -validation results showed that the constructed pixel scale AGB estimation had good robustness, with an average R^2 of 0.83 and RMSE of 34.13 g/m^2.

Our dataset provides an important input parameter for a comprehensive understanding of the role of ~~the~~ QTP in ~~the process of~~ global climate change processes. The dataset is available from the National Tibetan Plateau/Third Pole Environment Data Center (https://doi.org/10.11888/Terre.tpdc.272587, Zhang et al., 2022).

1 Introduction

Grasslands, accounting for approximately 37% of the earth's surface, play an essential role in global carbon cycling and food supply (O'mara, 2012). However, most natural grasslands have been degraded to a certain extent due to overgrazing, farmland encroachment, soil erosion, and global climate change (Suttie et al., 2005; Ramankutty et al., 2008; O'mara, 2012). Therefore, timely monitoring of grassland health is crucial for sustainable development and understanding ~~the~~ global carbon cycling processing. Aboveground biomass (AGB) is a key indicator of grassland status and an important input parameter for ~~the~~ ecological ~~model~~ modeling and carbon storage estimation. Thus, accurate and rapid estimation of AGB is valuable for grassland monitoring.

The advent of satellites has made it possible to map the spatiotemporal dynamics ~~of large areas~~ of grasslands over large areas. ~~The advent of satellites makes it possible to map the spatial distribution and temporal dynamics of grassland over large areas.~~ Spectral information from different satellites has been employed for biomass estimation, such as Sentinel-2, Landsat, and MODIS (Wang et al., 2019; Zhang et al., 2016). Although there are differences in spatial and spectral resolution, the core idea of building a biomass model is constructing the linear or nonlinear relationships between the ~~field~~ field-measured samples and various satellite spectral indices. Therefore, the estimation accuracy is closely related to the quality and quantity of ground samples (Morais et al., 2021; Yu et al., 2021). However, t~~T~~here are still two deficiencies in ground data ~~collection~~acquisition: the large spatial ~~scale~~ gap between the traditional samples and satellite pixels, and the low efficiency.

How to narrow the spatial gap between traditional samples and satellite pixels is an urgent problem to be solved. Since it is impossible to harvest all ~~the~~ grasses within a pixel range, ~~an~~ the average of 3-5 quadrats ~~size samples~~ (0.5 m × 0.5 m or 1m × 1m) is usually used as the measurement (Dusseux et al., 2015; Yang et al., 2017), which results in a considerable spatial gap. A lot of studies have been carried out to upscale ground measurements to satellite pixels (Crow et al., 2012; Bian and Walsh, 1993), such as block Kriging geostatistical interpolation, different types of regression models, or machine learning algorithms (Cheng et al., 2007; Wang et al., 2014; Cannavacciuolo et al., 1998; Dancy et al., 1986; Li et al., 2018). However, the accuracy of these methods depends on the density of sampling points. In addition, fine-resolution satellites were used as a bridge to reduce the impact of scale mismatch on AGB estimation (Yu et al., 2021; He et al., 2019). The reason is that the finer the satellite resolution, the smaller the spatial gap with the ground samples ~~The primary reason is that the spatial gap between traditional ground data and fine-resolution satellites is much smaller than medium or coarse-resolution satellites~~ (Wang and Sun, 2014; Morais et al., 2021). Therefore, obtaining ~~a value~~ground samples that match~~hing~~ the pixel scale is the key to ~~improving~~ improving the accuracy of~~the~~ satellite AGB ~~inversion~~estimation ~~using remote sensing data~~ ~~accuracy from remote sensing~~.

Improving the efficiency of ground sampling is ~~the other problem to be solved~~ another issue that needs to be addressed. Although the ~~the~~ traditional ~~field~~ sampling method can ~~get~~ yield ~~high~~ high-accuracy results, it is time-~~-~~consuming and labor-intensive. ~~Large-region grassland AGB inversion often requires years of accumulation to obtain ground observation samples with sufficient spatial representation.~~ For example, ~~it took~~ Yang et al. spent five years ~~to complete~~completing the collection of ground samples to ~~investigate~~ invert the grassland AGB ~~in~~ in China (Yang et al., 2010). Moreover, with limited original ground data, some scholars had to use~~expanded the sample size by using~~ the data published by others~~-~~ to expand the sample size ~~when the original ground data was limited~~ (Xia et al., 2018; Jiao et al., 2017). However, datasets from different sources may affect the overall accuracy due to the differences in sample plot size, sample size, and sampling methods.~~Considering the differences in the plot area, quadrat size, and sampling method, datasets from different sources may affect the overall inversion accuracy.~~

The development and ~~popularization~~ popularity of unmanned aerial vehicle (UAV) technology has ~~provides~~ provided new ~~ideas for to solving solve~~ solutions to the above problems. UAV images have been successfully used to estimate ecological ~~indicators~~ metrics such as FVC, biomass, and canopy height (Chen et al., 2016; Zhang et al., 2018; Bendig et al., 2015). The use of UAVs has the following unparalleled advantages over traditional sampling methods. ~~Compared with traditional sampling methods, the use of UAVs has the following incomparable advantages.~~ First, UAVs can effectively obtain ~~2D~~ two- or ~~3D~~ three-dimensional vegetation information ~~about vegetation structure~~ in a non-destructive way ~~without destroying damaging it~~, which is ~~helpful~~ helpful for grassland ~~the~~ estimation ~~of grassland biomass~~ (Lussem et al., 2019; Zhang et al., 2022a; Zhang et al., 2018). Second, UAVs can ~~easily~~ rapidly collect key parameters of grassland within satellite pixels (e.g., FVC, Chen et al. 2016). Hence, UAV images can serve ~~be used~~ as a bridge to reduce the spatial gap between ~~the~~ field samples and ~~the~~ satellite pixels. However, most current UAV-based grassland biomass estimations are small-scale, ~~with~~ with few regional-scale studies. W~~It is still unknown w~~hether UAVs can be used to ~~narrow~~ reduce the spatial gap between ~~the~~ traditional ground ~~samples~~ sampling and satellite pixels remains an open question. In addition, ~~due to the limited sample size,~~ previous studies ~~regional-scale grassland AGB models~~ lacked ~~independent years of~~ cross-year validation~~cross-validation~~ to test the robustness of the AGB estimation model over time due to the limited sample size~~in different periods~~.

This study proposed a new ~~method~~ approach that ~~combining~~ combines traditional ground sampling, UAV ~~photographing~~photography, and satellite data to ~~generate~~ produce a new reliable AGB dataset of QTP grassland. The objectives of this study were: 1) to construct a ~~the~~ UAV-based grassland AGB estimation model~~s~~ at the quadrat/satellite pixel scales, respectively; 2) to investigate whether UAVs can be used as a bridge to ~~narrow~~ reduce the spatial gap between

~~traditional~~ ground ~~observation~~ samples and satellite pixels~~, and~~ to improve the ~~estimation~~ accuracy of grassland AGB~~;~~, and 3) to map the AGB of alpine grasslands on the Qinghai-Tibetan Plateau (QTP) from 2000 to 2019.

2 Materials and Methods

2.1 Study Site

QTP is the highest and largest plateau on the earth (26°00′12″~39°46′50″N, 73°18′52″~104°46′59″E), with an average elevation of ~4000 m and an area of approximately 257.24×10^{4} km^{2} (Figure 1). It is located in western ~~western~~ China, ~~and th~~with an average~~e~~ annual ~~average~~ temperature and precipitation of about ~~are around~~ 1.6℃ and 413.6 mm, respectively. The main grassland types are alpine meadows, alpine steppe, and sparse grassland, which play a critical role in climate regulation, water conservation, and biodiversity protection (Ding et al., 2013). ~~However, grassland ecosystems are fragile and vulnerable to global climate change and human activities, and have high spatial heterogeneity.~~ In this study, the boundary of the QTP of China (Zhang et al., 2014) was downloaded from the National Earth System Science Data ~~-~~Center~~r~~, National Science & Technology Infrastructure of China (http://www.geodata.cn(Zhang et al., 2014)). ~~The~~ G~~g~~rassland type data was derived from the 1:1000000 Chinese digital grassland classification map provided by the China ~~r~~Resource and ~~e~~Environmental ~~science~~ Science and ~~data~~ Data C~~c~~enter ~~of China~~ (https://www.resdc.cn/). This data set, generated through field surveys in the 1980s and supplemented by satellite and aerial imagery, is the most detailed grassland-type map available.~~This data set was produced through field surveys and supplemented by satellite and aerial images in the 1980s and is also the most detailed map of grassland types.~~ For comparison with others ~~studies~~, we combined the grassland types into three categories: alpine meadow, alpine grassland, and sparse grassland, and resampled ~~them~~ to 250 m~~eters~~ (Table A1).

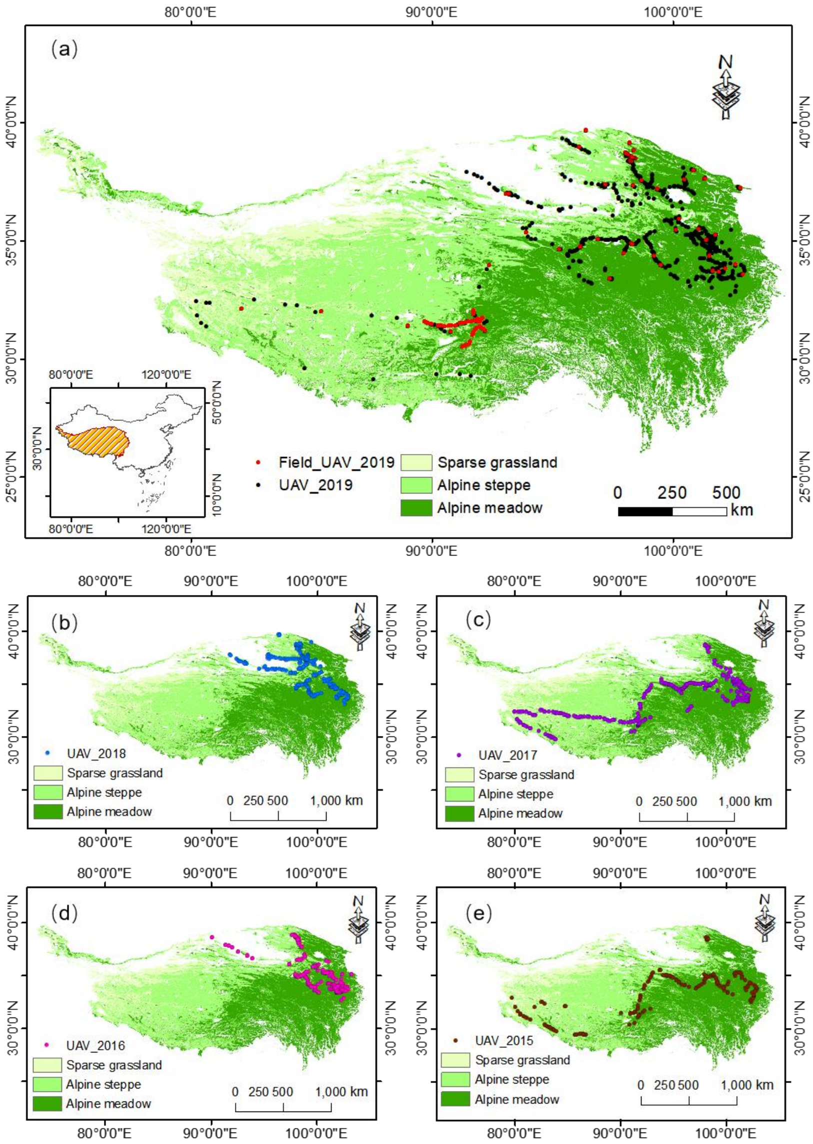

Figure 1. Distribution of field and UAV sampling sites ~~of~~in -2019 (a); ~~and~~ UAV sampling sites in ~~-of 2015-2018 in~~ alpine grasslands on the QTP from 2015-2018 -(b-e). Field_UAV_2019 represents the quadrat~~-~~-scale sampling sites ~~for~~ for the 2019 ~~2019~~ UAV-Field synchronous grassland biomass experiment. UAV_year represents the UAV sampling point based on the GRID or RECTANGE mode of the corresponding year.

2.2 Overall technology roadmap

Figure 2 ~~shows~~was the ~~The~~ overall flowchart of this study~~of UAV-field investigation and the construction of grassland AGB estimation model at different spatial scales were shown in Figure 2,~~ . ~~which~~ It consisted ~~s~~ of ~~mainly includes~~ four main steps: 1) UAV and field investigation; 2) ~~constructing~~ constructing the ~~the grassland~~ AGB estimation model at the quadrat scale; 3) upscaling the grassland ~~the~~ AGB to the MODIS pixel scales; 4) building the ~~the final~~ AGB estimation model at the MODIS pixel scale and applying it to the QTP region. More detailed information ~~about~~ on each step ~~was~~ ~~is~~was described in the following sections.

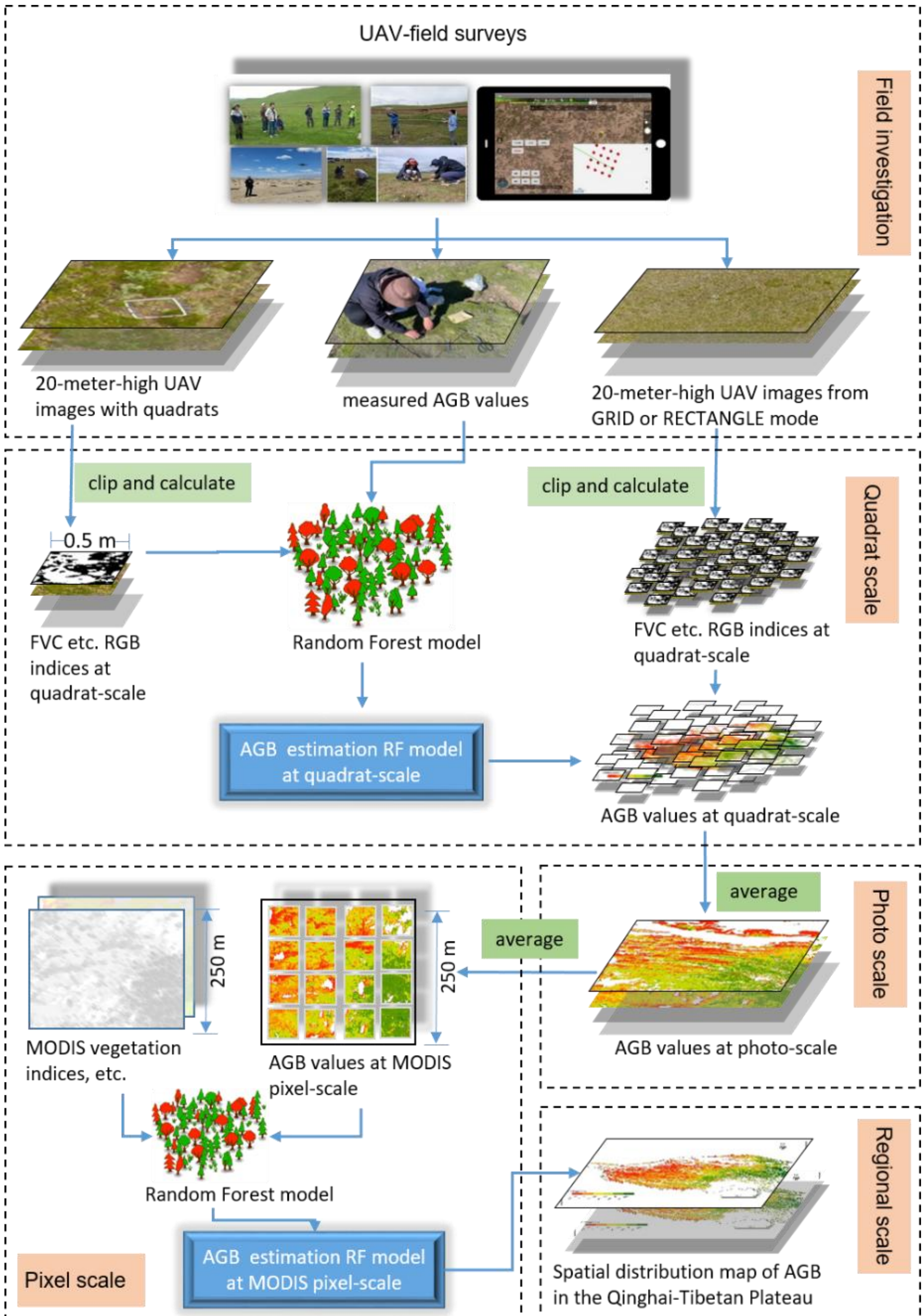

Figure 2. The overall flowchart of UAV -field ~~investigation~~ survey and the construction of grassland AGB estimation models at different spatial scales.

2.3 Field investigation

2.3.1 UAV and route planning

DJI Phantom 3 ~~professional~~ Professional (DJI Company, Shenzhen, China), a popular consumer quadrotor UAV ~~equipped~~ with a high-resolution RGB camera, was used to collect UAV images of the QTP from 2015 to 2019. It has a 1/23-inch CMOS sensor and is capable of taking 12-megapixel photos. In addition, it uses a 3-axis stable gimbal to take photos ~~downward~~ vertically downward ~~and~~to eliminate the distortion of UAV images. It has good environmental adaptability, with an operating~~the working~~ temperature range~~s~~ from 0° to 40°, ~~,~~and a maximum ~~the highest~~ take-off altitude ~~can reach~~ of 6000 meters. Therefore, ~~it~~it is well ~~can adapt~~adapted ~~well~~ to the low temperature and high altitude of the QTP. More detailed information about the UAV system ~~is~~ was listed in Table A2.

Fragmentation Monitoring and Analysis with aerial Photography (FragMap) system, ~~which can realize~~ capable of long-term collaborative observation, was used for UAV route planning (Yi, 2017). ~~The repeatability of UAV observation is the basis for understanding the ecological process. Through~~ During 2015-2019, we conducted UAV monitoring of the QTP grasslands using FragMap ~~(Fig. 1).~~~~FragMap, we conducted UAV observations on the QTP from 2015 to 2019~~ (Figure 1). Over 2,000 fixed flight routes were set~~-~~ up during this period,~~during this period ,~~ and more than 37,000 UAV images were collected, providing a reliable UAV data~~-~~set for this study (Table 1).

Table 1. UAV sampling information from 2015 to 2019

Year	Flight Mode	Number of routes	Photo number	Acquisition time
2015	RECTANGLE	214	2568	7.05 ~8.24
2016	RECTANGLE	334	4008	6.20~9.29
	GRID	150	2400	6.20~9.23
2017	RECTANGLE	315	3780	5.10~10.24
	GRID	322	5152	7.15~8.22
2018	RECTANGLE	79	948	7.22~8.03
	GRID	303	4848	7.04~8.29
2019	GRID	885	14160	7.12~9.21
	Total	**2602**	**37864**	

GRID, RECTANGLE, and BELT are the most commonly used flight modes in the FragMap software. ~~The~~ GRID and RECTANGLE modes have 16 and 12 waypoints for capturing UAV images within a MODIS pixel range (Figure A1). Their flying height and speed are set to 20 m and 3m/s, respectively. The spatial coverage of a 20-meter-high UAV photo is about 26 m × 35 m. The BELT mode is similar to GRID, but is designed to obtain ~~get~~ near-ground UAV image data with ~~a~~ higher resolution (Figure 3b). It can be combined with the traditional sampling method to ensure the ~~that~~ consistency of UAV images ~~are consistent~~ with the ground ~~quadrats~~ samples (Figure 3d). ~~Generally~~Typically, the BELT size is set to 40 m × 40 m, and the flying height and speed are set to 2 m and 1 m/s to ensure that field ~~workers~~ crews have enough time to place ~~a~~ sampling ~~quadrat~~ frames ~~on~~ under the UAV ~~shooting~~ waypoints. As with the GRID mode, 16 UAV images can be captured ~~during~~ in a single ~~one~~ flight. Compared with the MOSAIC flight ~~flight~~ mode (which requires a guaranteed overlap rate between photos to obtain a full view of an area), our design is more in line with the traditional ecological sampling concept. It allows for a better balance of spatial representation and accessibility of samples, resulting in efficient sample collection.

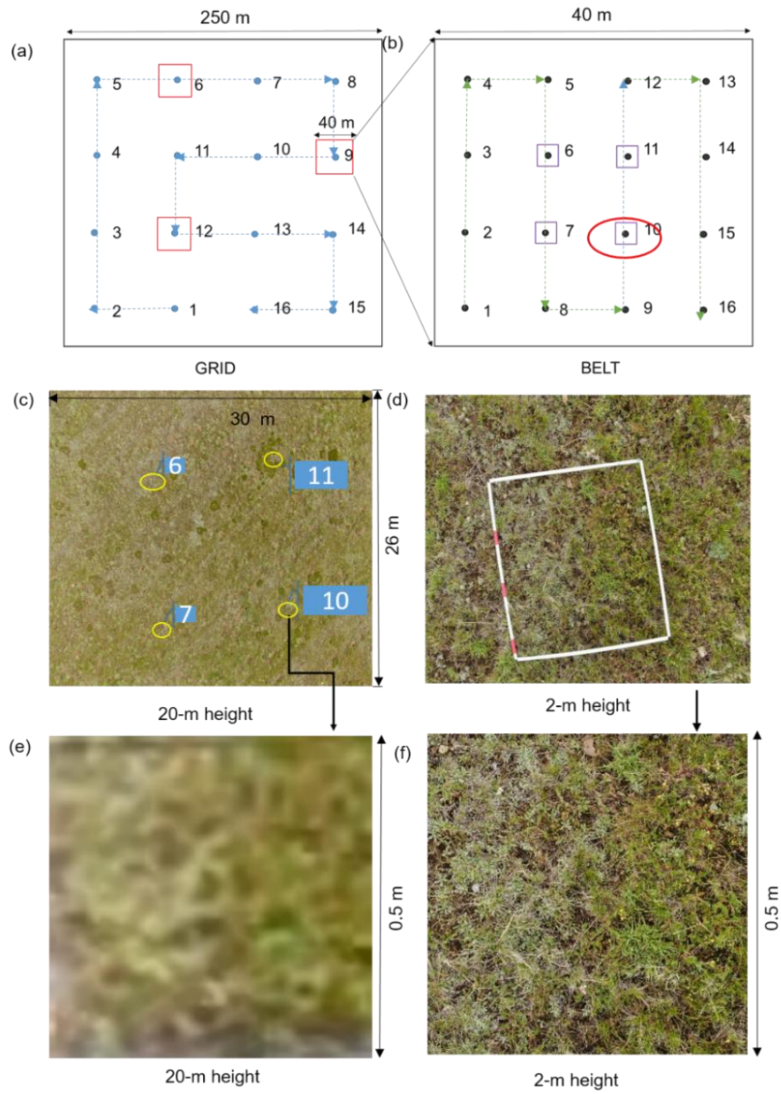

Figure 3. Schematic diagram of the UAV-field synchronization experiment in 2019: a combination design of GRID (a) and BELT (b) flight modes; a UAV image with a quadrat from the BELT mode at the height of 2 m (d); a 20-meter-high UAV image including four sample quadrats (c); and the cropped UAV images at quadrat scale from 20 m (e) and 2 m (f) height, respectively.

2.3.2 Synchronization experiment of UAV and field sampling

A UAV-field biomass synchronization experiment was designed in 2019 to ensure spatial matching ~~among~~ ~~between~~among satellites, UAVs, and ground sampling (Figure 3). The specific implementation steps were as follows. First, we set a GRID flight mode with ~~the~~ a MODIS pixel size (250 m × 250 m) (Figure 3a). Then, three waypoints were randomly selected from the GRID ~~route~~ mode ~~were randomly selected for~~ to set ~~setting~~ the BELT flight ~~routes~~ modes (40 m × 40 m). For each BELT, ~~we placed~~ a sampling ~~quadrat~~ frame (0.5 m × 0.5 m) was placed at its 6, 7, 10, and 11 waypoints to ensure that the

GRID image ~~can~~ could contain the four ~~quadrats~~ frames ~~described~~ mentioned above (Figure 3b-c). Then, at the end of all flights, the g~~G~~rassland AGB samples were ~~then~~ cut, bagged, and numbered ~~at the end of all flights~~. Finally, these samples were oven-dried at 65℃ to constant weight to obtain the field-measured AGB values.

2.4 Data processing

2.4.1 UAV photo pre~~-~~processing and indices calculation

~~The UAV photo pre~~Pre-processing of UAV photos included image quality inspection, ~~image~~ cropping, and calculation of different indices~~.~~. First, we eliminated ~~the~~ overexposed or ~~blurry~~ blurred 20-meter-high UAV images. Second, the pixels in the sampling ~~quadrat~~ frames were cropped and saved (Figure 3e). Third, ~~we calculated~~ the RGB indices for the cropped UAV images were calculated. Similar to our previous study, indices included color space, histogram, and vegetation indices, the details of which ~~could~~ can be found in Zhang et al. (2022a). ~~reference (Zhang et al., 2022a).~~ In addition, 30 other RGB vegetation indices were added as candidate independent variables. The names, formulas, and references of the above indices~~were~~ were shown in Table A3.

2.4.2 MODIS vegetation index and other spatial data

The MOD13Q1(v006) product was downloaded from the NASA earth explorer website (https://earthexplorer.usgs.gov/) for ~~the~~ inversion of the alpine grassland AGB on the QTP. The data ~~contained~~ contained two commonly used vegetation indices, the N~~n~~ormalized ~~vegetation~~ Vegetation ~~index~~ Index (NDVI) and the ~~enhanced~~ Enhanced ~~vegetation~~ Vegetation ~~index~~ Index (EVI), with spatial and temporal resolutions of 250 m and 16 days, respectively. A total of 2,842 scenes from 2000 to 2019 were downloaded. Then, the MODIS images were reprojected and stitched using the MODIS ~~projection~~ Projection ~~tool~~ Tool (MRT). After that, the corresponding vegetation indices closest to the time of the UAV sampling were extracted to construct/validate a pixel-scale AGB estimation model ~~to construct a pixel-scale AGB estimation model~~. ~~After that, we used the point extraction function in ArcGIS software to get the corresponding vegetation indices of the UAV samples to construct the pixel-scale AGB estimation model.~~ In addition, ~~based on the NDVI index and the formula kNDVI= TANH (NDVI^2),~~ the kNDVI index was calculated to overcome the NDVI saturation issue based on the equation kNDVI= TANH (NDVI^2) (Camps-Valls et al., 2021). The annual maximum vegetation indices were calculated by the maximum value composition (MVC) algorithm ~~of ENVI software~~ to estimate the spatial AGB distribution of QTP from 2000 to 2019 (Holben, 1986; Wang et al., 2021; Gao et al., 2020).

Furthermore, ~~the~~ meteorological, soil texture~~,~~ and topographic data were also included as candidate independent variables for constructing the pixel-scale AGB estimation model. Meteorological factors, including ~~the~~ annual mean temperature (TA), annual mean precipitation (PREC), and annual total solar radiation (RAD), were calculated based on the daily meteorological dataset from the National Meteorological Information Center of China. The data processing steps mainly included interpolation, cumulative summation, and annual averaging ~~processing~~ to obtain ~~the~~ a meteorological raster dataset with a spatial resolution of 1000 meters (Li et al., 2021). Moreover, ~~the spatial distribution data of~~ soil texture data ~~with~~ ata ~~1~~ 1 km spatial resolution, including the ratio of soil organic matter (SOM), clay, sand, and silt, were downloaded from the Resource and Science and Data Center of China (https://www.resdc.cn/). All the meteorological and soil datasets were resampled into 250 m by ArcGIS software to match the MODIS data.

Terrain factors included the digital elevation model (DEM), slope, and aspect. The DEM was derived from ~~shuttle~~ Shuttle ~~radar~~ Radar ~~topography~~ Topography ~~mission~~ Mission (SRTM) ~~images~~ imagery (version 004, 90 m) and resampled to 250 m. ~~Then use the terrain analysis tool of ArcGIS software to calculate the~~ The slope and aspect data were derived ~~based on~~from DEM data using the terrain analysis tool of ArcGIS software.~~Slope and aspect were then calculated from the DEM data using the terrain analysis tools of ArcGIS software.~~

2.5 AGB modeling and computation at different scales

We estimated the grassland AGB at three scales: the quadrat scale, the photo scale, and the satellite pixel scale (Figure 4). More detailed information ~~was~~~~is~~was described as follows.

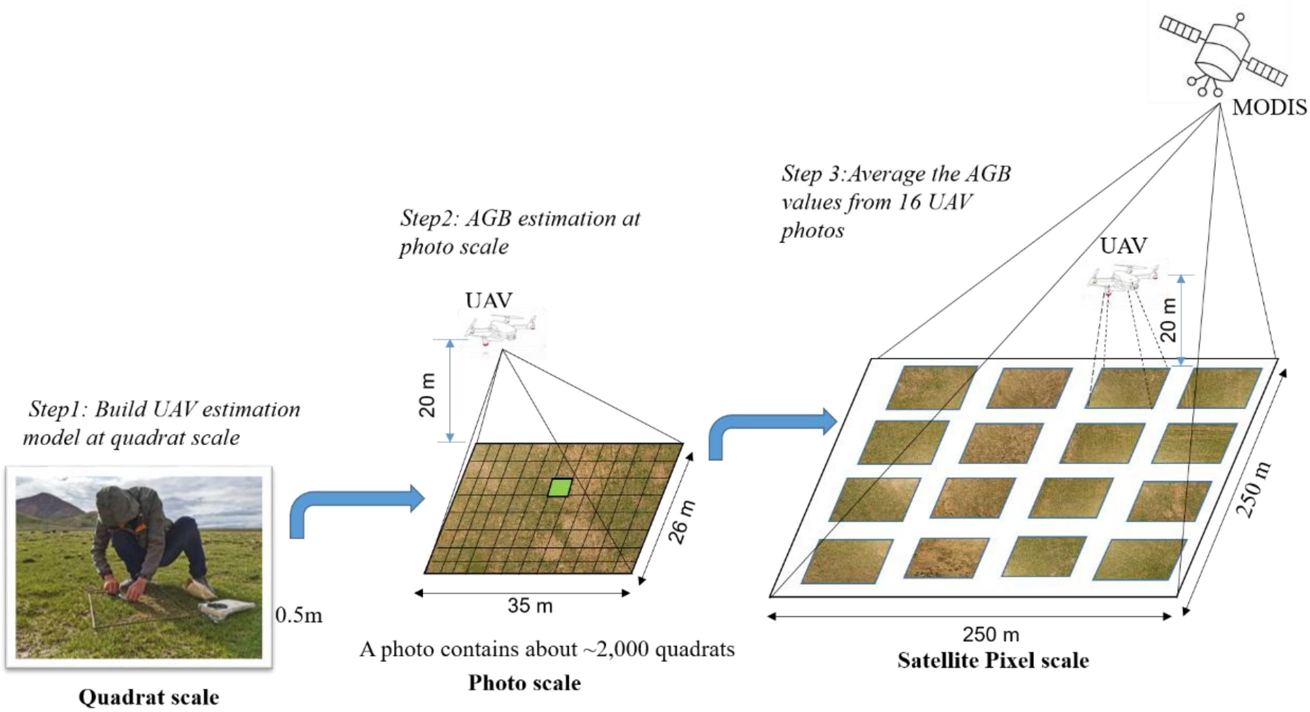

Figure 4. Upscaling steps to estimate grassland AGB matching the MODIS pixel scale.

2.5.1 Modeling method

Random Forest (RF) ~~(Breiman, 2001),~~ (Breiman, 2001) is an ensemble-learning algorithm~~, was~~ that has been widely used ~~employed~~ to estimate AGB ~~at different scales~~ due to its excellent performance ~~in biomass estimation~~ (Ghosh and Behera, 2018; Mutanga et al., 2012; Wang et al., 2016). The t~~T~~wo main parameters, namely the number of regression trees in the forest *(ntree*) and the number of feature variables required to create branches (*mtry*), were first optimized based on the root mean square error (RMSE) of training data ~~at first~~. Here, the value of *ntree* ~~values were~~was ~~tested~~ set from 100 to 5000 with an interval of 100, ~~and~~ while ~~the~~ *mtry* was set as the square root of the number of training sample features. In addition, the importance of each predictor was ranked by calculating the percentage increase in mean square error (%IncMSE).

The backward feature elimination method (BFE) was used to reduce the number of input variables to ~~simply~~ simplify the RF model (Vergara and Estévez, 2014). The main steps were as follows: 1) constructing an AGB RF model by including all predictor variables in the initial stages and calculating the %IncMSE index for each variable; 2) eliminating the least promising variable and then rerunning the RF model until only one independent variable was ~~was~~ left. Moreover, the corresponding coefficient of determination (R^2) and the corresponding RMSE were calculated in each iteration； 3) ~~selecting~~ the smallest subset of variables with the highest R^2 was selected as the final optimized indices.

In addition, different training and validation strategies were used at different scales. At the quadrat scale, a 10-fold cross-validation method was used due to the limited ground samples (Kohavi, 1995). At the pixel scale, 30% of the UAV-estimated AGB samples in 2019 were randomly selected as an independent validation dataset due to the large sample size. Meanwhile, the UAV_AGB values from 2015 to 2018 were used for cross-year validation ~~was performed using UAV-estimated AGB values estimated by UAVs from 2015 to 2018~~ to test the robustness of the model ~~over~~ over time~~different periods~~. Statistical ~~measures~~metrics~~, including~~ ~~the~~ R^2 (Eq.1) and ~~, the~~ RMSE (Eq.2) ~~, and mean absolute percentage error (MAPE, Eq.3),~~ were used to ~~qualify~~ evaluate the ~~model~~ performance ~~performance~~of the model.

$$R^2 = 1 - \frac{\sum_{i=1}^{n}(\hat{y}_i - y_i)^2}{\sum_{i=1}^{n}(\hat{y}_i - \bar{y}_i)^2} \quad (1)$$

$$RMSE = \sqrt{\frac{\sum_{i=1}^{n}(\hat{y}_i - y_i)^2}{n}} \quad (2)$$

where n is the number of samples, y_i and $\hat{y}_i$ represent the measured and the predicted AGB value, respectively, $\bar{y}_i$ is the mean value of measured AGB samples.

2.5.2 AGB RF estimation model at the quadrat scale (0.25 m^2)

Since the spatial coverage of a 20m-high UAV photo (26 m×35 m) is much wider than a single 2m-high UAV photo, making it easier to match to the MODIS pixel scale. Hence, the 20m-high UAV photos containing the sample frames were chosen for constructing the quadrat-scale AGB estimation model. A total of 906 pairs of quadrat-scale UAV-field AGB observation data were collected, with good spatial representativeness (Figure 1 a, red dots). The observed AGB values ranged from 0 ~~g/m^2~~ to 450 g/m^2, with mean and median values of 59.75 g/m^2 and 33.04 g/m^2, respectively, most of which were less than 100 g/m^2 (Figure 5a). ~~Then, the~~The cropped 20-meter-high UAV image indices and the measured AGB values were used as the independent and dependent variables to build the RF model (Figure 2).

2.5.3 AGB calculation at the photo scale (~900 m^2)

The steps ~~for~~ for AGB estimation of the ~~entire~~ whole 20-meter-high UAV photo were as follows: 1) First, each UAV photo was divided into ~2,000 quadrat-sized small patches. 2) Second, the AGB of each small patch was calculated based on the quadrat-scale AGB estimation model. 3) Finally, the average ~~value~~ of all ~~the~~ small patches was calculated as the AGB of the whole photo. Based on the above steps, the AGB values of 37,487 images in GRID or RECTANGLE mode were calculated using ~~over~~ more than 74 million AGB values ~~at the~~ of the quadrat scale (Table 1).

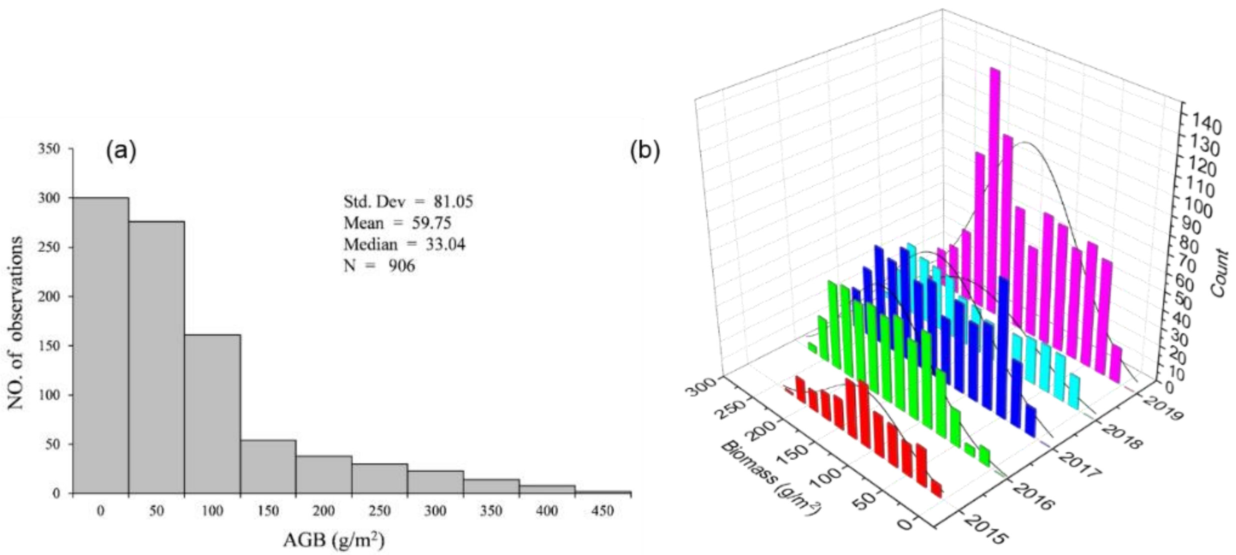

Figure 5. Histograms of field-measured AGB values at quadrat scale (a) and UAV-estimated AGB values of different years at the photo scale (b).

2.5.4 AGB RF model construction at MODIS pixel-scale (6,2500 m^2)

The following steps were involved in constructing the AGB estimation model at the pixel scale. 1) Since the coverage of a GRID or RECTANGLE ~~route~~ mode was similar to that of ~~the~~ a MODIS pixel, the average of its 16 or 12 photos was taken as the AGB value of the corresponding pixel. From 2015-2019, a total of~~–~~ 2,602 UAV-estimated AGB samples were obtained at the pixel scale ~~from 2015 to 2019~~ (Table 1). 2) The MODIS vegetation indices and other spatial metrics corresponding to each GRID or RECTANGLE ~~route~~ mode were then extracted using the ArcGIS software. Here, the MODIS NDVI, EVI, and kNDVI indices closest to the sampling time were chosen to minimize the time difference between sampling and satellite overpass.3) Subsequently, the UAV-estimated AGB values and the extracted spatial indices were used as dependent and independent variables to build the AGB estimated model at the pixel scale using the RF algorithm.

2.6 Uncertainty analysis

Since the actual AGB values of MODIS pixels cannot be directly obtained, vegetation indices were used to quantify the uncertainty of different AGB estimation methods. In other words, the higher ~~correlation between the estimated AGB and MODIS vegetation indices, the higher accuracy of~~the correlation between the estimated AGB and MODIS vegetation indices, the more accurate the estimation model was ~~was~~. ~~This stud~~ The performance of the estimation model was evaluated through ~~the~~ three aspects. In this study, we~~y~~ first~~ly~~ compared the correlation between the MODIS vegetation indices and AGB values obtained by traditional sampling and UAV estimation methods. We also explored the uncertainties of UAV sampling coverage by randomly combining the number of photos in a MODIS pixel, and tested whether the estimated AGB was closer to the true value as the number increased. Furthermore, the AGB validation results from GRID or RECTANGLE at the pixel scale were compared to understand the uncertainties caused by different flight modes.

2.7 Trend analysis of grassland AGB

This study combined the Theil-Sen median trend analysis and Mann-Kendall test to analyze the temporal variation characteristics of grassland AGB of QTP (Jiang et al., 2015). Theil-Sen median trend analysis is a robust trend statistical method with high computational efficiency, insensitive to outliers (Hoaglin et al., 1983). The Mann-Kendall test is a nonparametric test for time series trends, which does not require the measurements to follow a normal distribution and is not affected by missing values and outliers. The Theil-Sen Median trend analysis and Mann-Kendall trend test have been widely used to analyze vegetation index, cover, and biomass (Gao et al., 2020; Jiang et al., 2015; Fensholt et al., 2009). The formulas for the Theil-Sen median trend analysis and the Mann-Kendall method are detailed in Jiang et al. (2015)~~(Jiang et al., 2015)~~.

3 Results

3.1 Independent variables selected for AGB modeling

The ~~selected~~ independent variables for AGB estimation at the quadrat and pixel scales ~~were~~ ~~are~~were ~~listed~~presented in Table 2. A total of 36 independent variables were ~~finally~~ selected at the quadrat scale, including 26 vegetation RGB indices, 6 histogram indices, and 4 color space indices (Figure A2). At the pixel scale, five variables were selected, including NDVI, kNDVI, EVI, PREC, and DEM (Figure A3).

Table 2: Selected independent variables for the AGB modeling at quadrat and pixel scales. The full names of each variable at the quadrat scale were listed in Table A3~~2~~.

Scale	Model	Number	Independent variables
Quadrat	RF_Q	36	FVC, WI, GI, EXG, TGI, EXGR,VEG, GRATIO, COM, CIVE, RGBVI, EXR, GLA, GRRI, MVARI, MGRVI, GRVI, RGRI, GBRI, VARI, NDI, RRATIO, EXB, V, IPCA, INT, HOC_R_CORR, HOC_B_CHIS, HOC_R_CHIS, HOC_G_CHIS, HOC_G_CORR, HOC_B_CORR B, H, G, R,
Pixel	RF_P	5	NDVI, kNDVI, EVI, DEM, PREC

3.2 Modeling and accuracy assessment

For ~~the quadrat-scale~~ the AGB estimation model at the quadrat scale, the results of 10-cross validations ~~results~~ showed that there was a significant linear relationship between the estimated ~~AGB values of the model~~ and the measured values (R^2=0.73, p<0.001, Table 3, Table A4). The student's t-test was also used to ~~evaluate~~ assess whether there was a significant difference~~s~~ ~~existed~~ between the predicted AGB values and the measured values at a ~~coefficient~~ confidence level of 95%. As shown in Table 4, ~~showed~~ there was ~~there was~~ no significant difference ~~between the predicted and measured average AGB values~~ (p=0.51>0.05) with an ~~. The total~~ RMSE of ~~and MAPE of the prediction model were~~ 32.94 g/m^2 ~~and 48.94%, respectively~~. The scatter plot showed that the model predicted well when the measured biomass was less than 150g/m^2, but showed some underestimation when it was ~~greater~~ more than 200g/m^2 (Figure 6a). ~~The reason might be that~~It may be because the number of samples ~~the sample size larger~~ more than 200g/m^2 ~~was~~ is relatively small, accounting for only 8.50% of all~~the total number of~~ samples (Figure 5a). Although the ~~UAV~~ sample size of UAVs varied ~~yearly~~from year to year, ~~the estimated~~ most of the AGB values ~~at~~ estimated from photos~~the photo scale~~ ranged from 0 to 300 g/m^2 (Figure 5b). ~~Th~~~~Most of the AGB averages estimated by UAVs were around 150 g/m² from 2016 to 2019, and slightly lower in 2015 (108 g/m²).e mean UAV AGB in 2016-2019 was around 150 g/m², while it was slightly lower in 2015 with 108 g/m².~~

For the pixel-scale AGB estimation model, there was a strong linear relationship ~~s existed~~ between the predicted AGB and UAV estimates ~~estimated values~~ for 2015-2019 (Table A4). ~~In 2019,~~The fitting coefficient R^2 was 0.85 ~~in~~ for 2017-2019~~, an,d~~ and slightly lower ~~in~~ for 2015-2016 at~~, at~~ 0.63 and 0.77, respectively (Table 3, Figure 6b-f). The RMSE ~~and MAPE~~ of the pixel-scale model ranged from 23.36 ~~g/m2~~ to 34.07 g/m^2 ~~, 12.32% to 25.19%, respectively~~ (Table 3). In addition, we found ~~that there were~~ no significant differences between the predicted and measured average AGB values ~~,~~ except ~~in~~ for 2017 and 2018 (Table 4). ~~While~~ While the average model projections ~~the averages fof~~ or ~~the~~ 2017 and 2018 ~~model estimates are~~ were 14.72% and 13.78% lower than the UAV estimates~~, respectively~~, they ~~are~~ were within ~~an~~ acceptable ranges.

Therefore,~~ the cross-year validation results indicated that~~ ~~it~~ the constructed pixel-scale AGB estimation model had ~~good~~ good performance and robustness in different ~~across~~ ~~in different~~ years~~ the cross-year validation results indicated that it had good performance and robustness in different years~~ (Figure 6b~f).

Table 3: Validation results of AGB models at quadrat and pixel scales

Scale	Year	Training set		Validation set	
		R^2	RMSE(g/m^2)	R^2	RMSE(g/m^2)
Quadrat-scale	2019	0.94	20.18	0.73 ***	32.94
Pixel-scale	2019	0.96	10.68	0.85 ***	23.36
	2018	__	__	0.85 ***	24.83
	2017	__	__	0.85 ***	23.83
	2016	__	__	0.77 ***	31.28
	2015	__	__	0.63 ***	34.07

'***' significant at $p<0.001$

Table 4: T-test results between the predicted and measured AGB values for the modes ~~of~~at the quadrat and pixel scales

Validation model	Measured mean	Predicted mean	t	df	p-value
2019_Quadrat-scale	51.57	54.35	-0.66	939.35	0.51
2019_Pixel_scale	136.68	137.7461	-0.15	340.78	0.88
2018_Pixel_scale	152.49	131.48	4.01	723.81	6.63e-05
2017_Pixel_scale	141.42	120.60	5.48	1225.2	5.26e-08
2016_Pixel_scale	149.56	142.70	1.68	961.99	0.09413
2015_Pixel_scale	108.65	98.23	1.96	1225.2	0.05

3.3 Correlation analysis between AGB values and MODIS indices

The correlation~~ss~~ between the UAV-estimated AGB values and MODIS vegetation ~~indices~~ indices were much better than the traditional ~~ground~~ sampling method (Figure 7a). For example, the correlation between NDVI and traditionally measured AGB was only 0.53, much lower than ~~that~~ that obtained from a single UAV image (r=0.74). Moreover, the correlation between NDVI and UAV-estimated AGB increased with the number of UAV photos. It increased rapidly as the number increased from 1 to 4 (from 0.74 to 0.86), then slowed down and stabilized (from 0.87 to 0.88).

In addition, we compared the ~~the~~ scatter plots and fitting lines between NDVI and different AGB estimation methods (Figure 7b-f). The results showed a weak linear relationship between the traditionally measured AGB and NDVI~~a weak linear relationship between the traditional measured AGB and NDVI~~, ~~and~~ with an ~~the~~ R^2 ~~was only~~of 0.29. With the UAV sampling method, ~~Linearity~~ the linear relationship was greatly improved ~~ausing the UAV sampling method a~~nd increased with the number of ~~photos~~photographs. The fit coefficient R^2 increased from 0.54 to 0.78, much higher than the traditional sampling method (Figure 7).

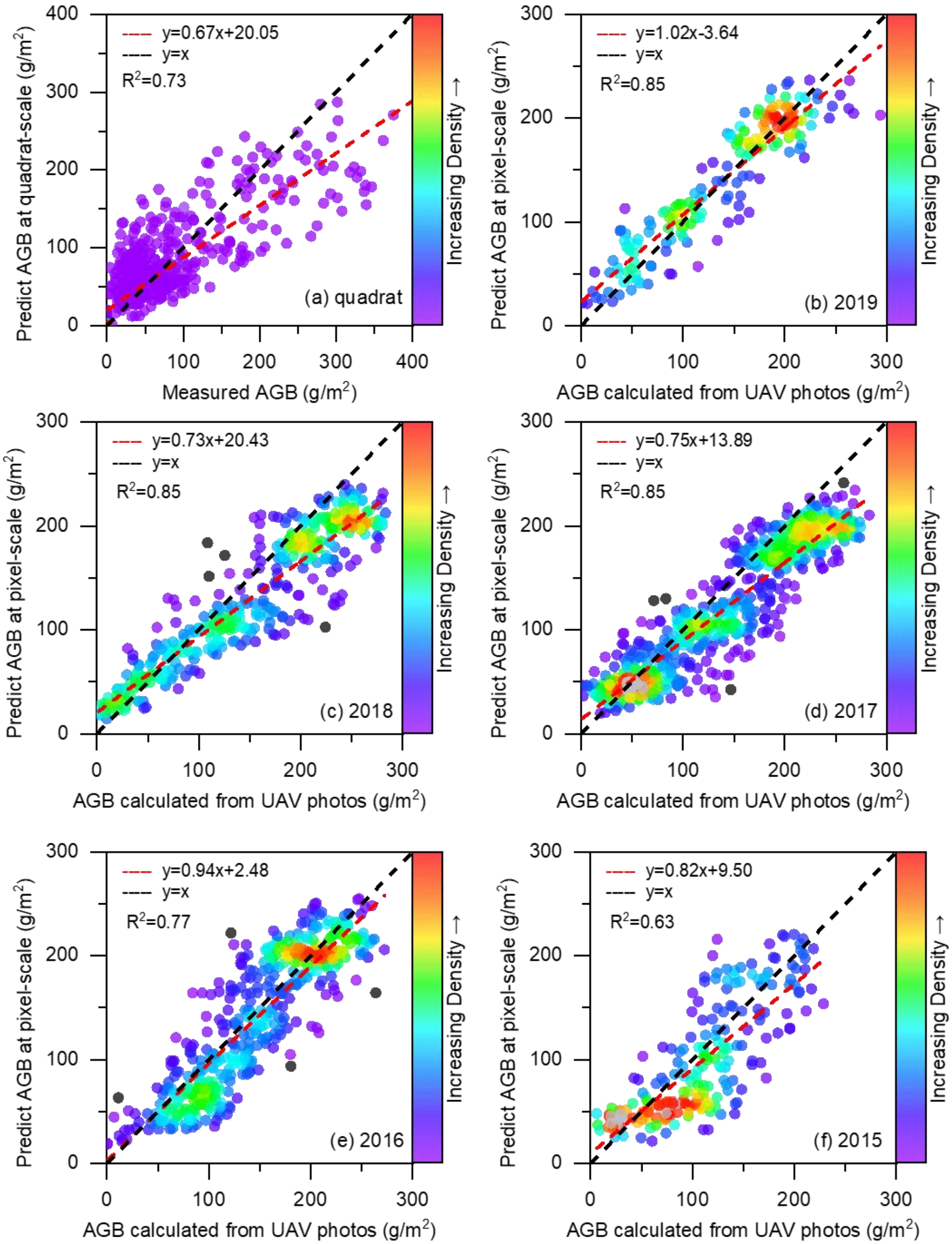

y=0.67x+20.05
y=x
R²=0.73
(a) quadrat
Predict AGB at quadrat-scale (g/m²)
Measured AGB (g/m²)
Increasing Density →
y=1.02x-3.64
y=x
R²=0.85
(b) 2019
Predict AGB at pixel-scale (g/m²)
AGB calculated from UAV photos (g/m²)
Increasing Density →
y=0.73x+20.43
y=x
R²=0.85
(c) 2018
Predict AGB at pixel-scale (g/m²)
AGB calculated from UAV photos (g/m²)
Increasing Density →
y=0.75x+13.89
y=x
R²=0.85
(d) 2017
Predict AGB at pixel-scale (g/m²)
AGB calculated from UAV photos (g/m²)
Increasing Density →
y=0.94x+2.48
y=x
R²=0.77
(e) 2016
Predict AGB at pixel-scale (g/m²)
AGB calculated from UAV photos (g/m²)
Increasing Density →
y=0.82x+9.50
y=x
R²=0.63
(f) 2015
Predict AGB at pixel-scale (g/m²)
AGB calculated from UAV photos (g/m²)
Increasing Density →

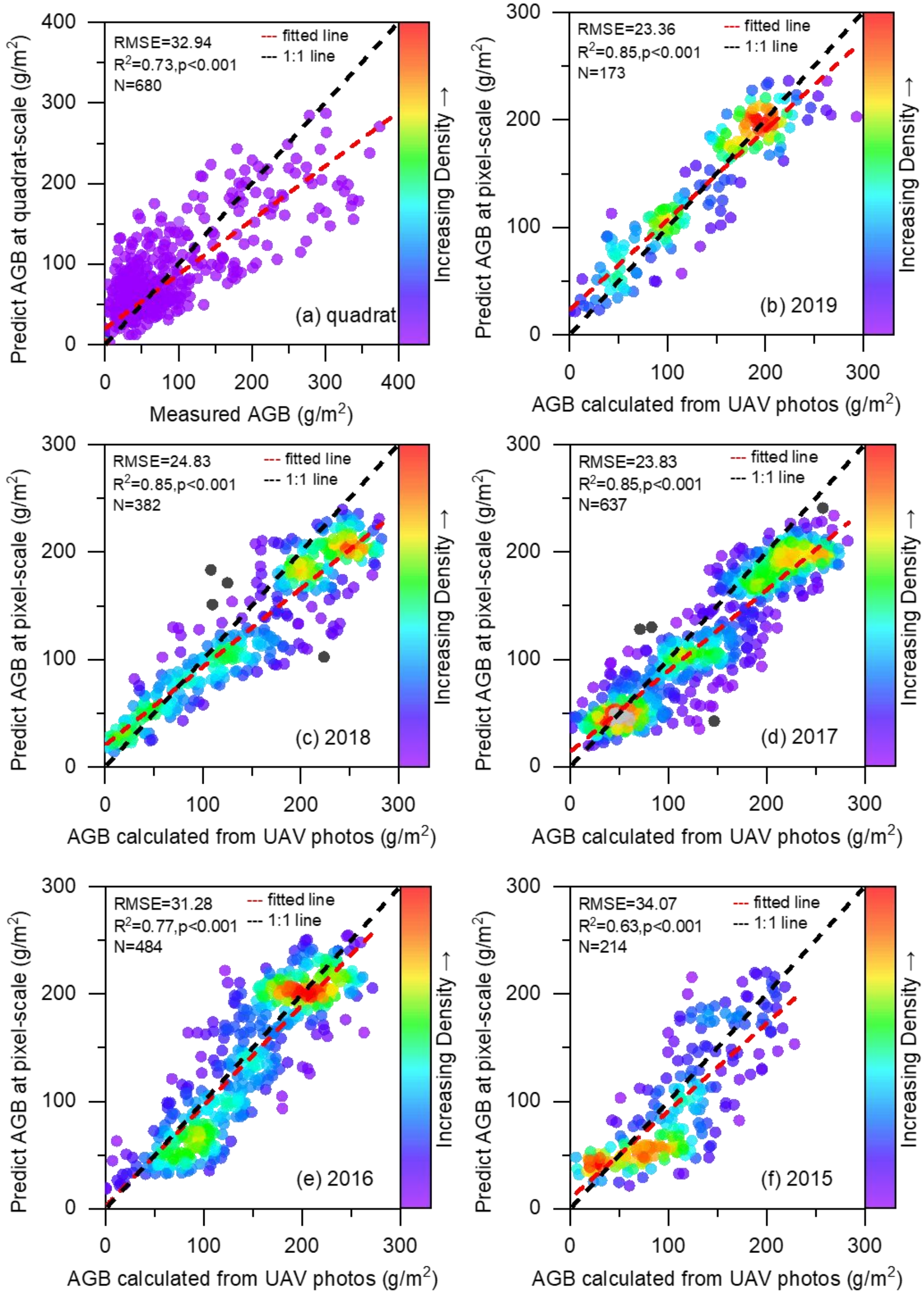

Figure 6~~Figure 6~~. Validation results of the AGB estimation models at the quadrat (a) and MODIS pixel scale for 2015-2019 (b~f).

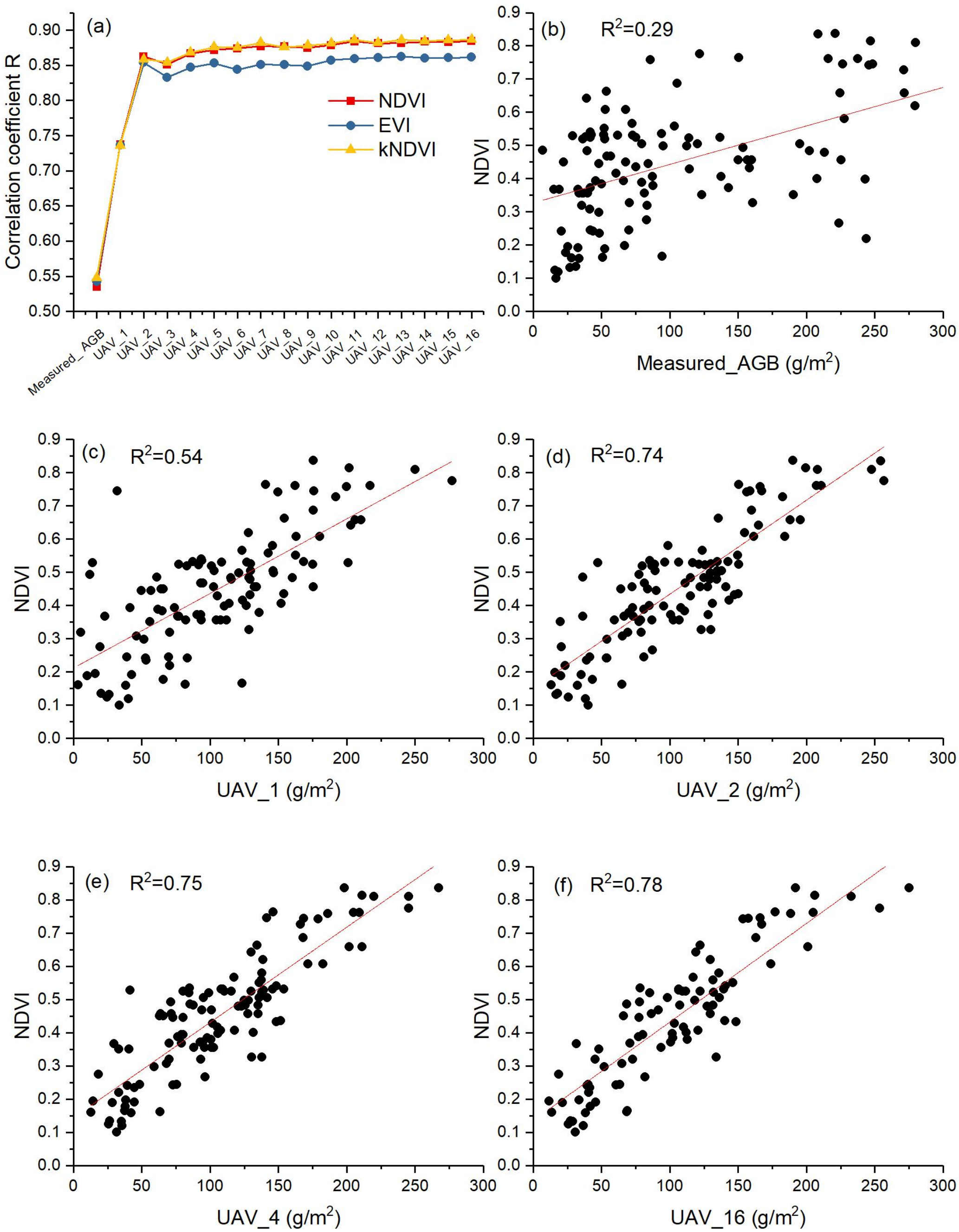

Figure 7. ~~The e~~Correlations between ~~the~~ MODIS vegetation indices and different AGB estimation methods (a); ~~the~~ scatter plots ~~between~~ of NDVI ~~and~~ with different AGB estimation methods (b-f). UAV_x, x represents the number of UAV photos used to estimate the average AGB at the MODIS pixel- scale. Here, ~~the value range of~~ x ~~is~~ ranges from 1 to 16.

3.4 Spatial distribution of grassland AGB

The spatial distribution of the average grassland AGB ~~on the~~on the QTP from 2000 to 2019 was calculated (Figure 8). The AGB gradually increased from west to east. As shown in Figure 8b, the average biomass of eastern OA1, IIAB, IB1, and IIC2 eco-geographical regions ranged from 150 to 190 g/m^2, and the average AGB of IC1 and IIC1 ranged from 80 to 110 g/m^2. The average AGB of IID2, IID3, IC2, and IID1 in the west was relatively low, ranging from 35 to 75 g/m^2. The ID1 region ~~is~~ was dominated by sparse grassland with the lowest average interannual AGB values, which fluctuated around 20 g/m^2 ~~with interannual mean AGB values fluctuating around 20 g/m^2.~~ (Figure 8b). ~~From 2000 to 2019,~~ ~~T~~the ~~mean~~average AGB ~~on the~~of QTP showed an insignificant increasing trend between 2000 and 2019, with an average growth rate of 0.22 gm^{-2}a^{-1} (Figure 9a). The overall mean AGB of the QTP was 103.6 g/m^2~~,~~, ~~and~~with 151.85 g/m^2, 60.85 g/m^2, and 28.91 g/m^2 for ~~the mean AGB of the~~ alpine meadow, alpine steppe, and sparse grassland, r ~~were 151.85 g/m^2, 60.85 g/, and 28.91 g/m^2,~~ ~~r~~respectively (Figure 9b). In addition, the temporal trend of grassland AGB in each pixel was analyzed. As shown in Figure 10, the IID3, ID1, IID2, and IIC2 eco-geographical regions of the northern QTP showed an increasing trend from 2000 to 2019, while the IC2, IB1, and IIC1 regions showed some degradation. Therefore, ~~although the overall AGB of the QTP showed an increasing trend from 2000 to 2019,~~ there was spatial heterogeneity in the temporal variation.

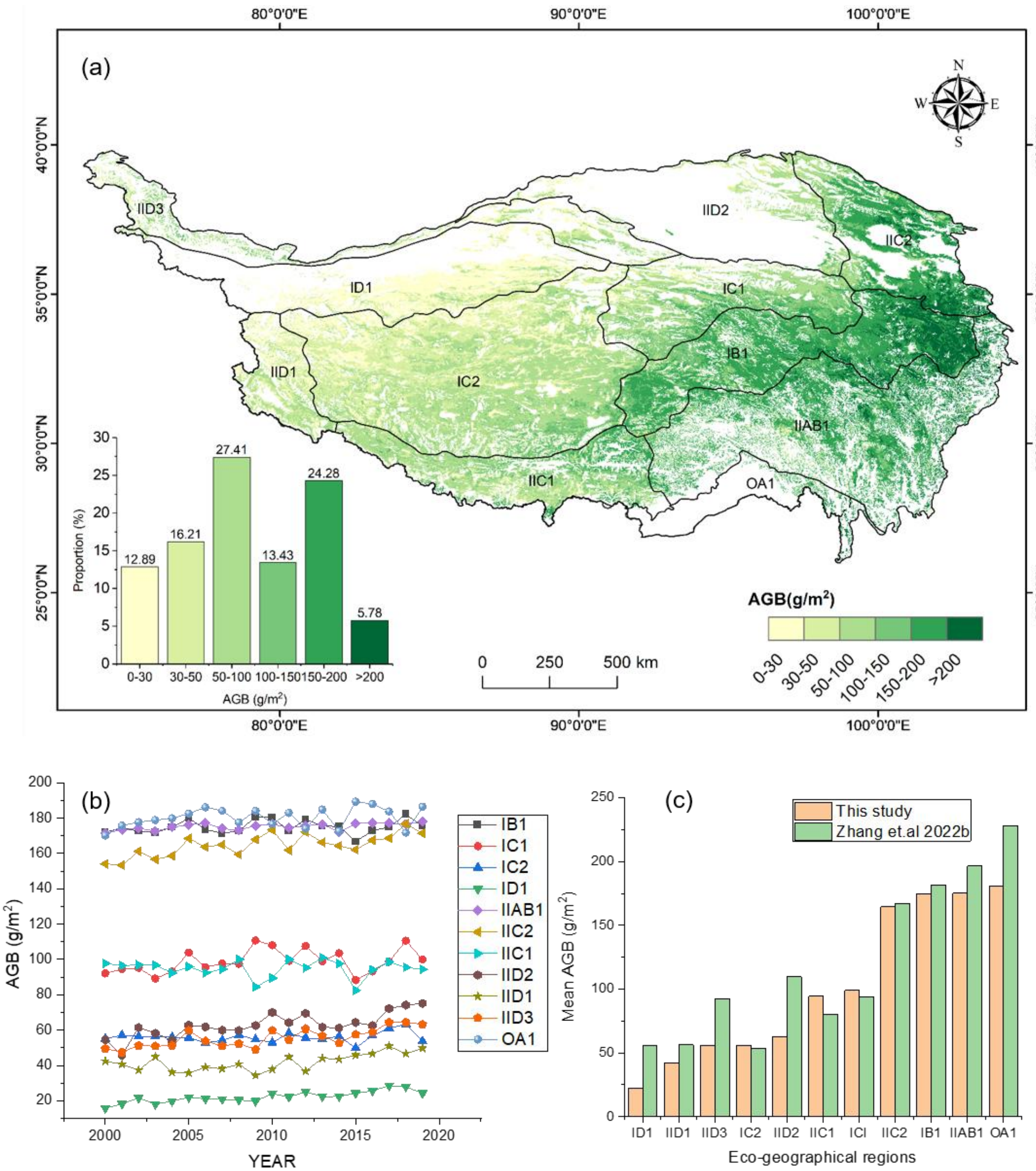

~~From 2000 to 2019, the mean AGB on the QTP showed an insignificant increasing trend, with an average rate of 0.22 gm^{-2}a^{-1} (Figure 9a). The overall mean AGB of the QTP was 103.6 g/m^2, and the mean AGB of the alpine meadow, alpine steppe, and sparse grassland were 151.85 g/m^2, 60.85 g/, and 28.91 g/m^2, respectively (Figure 9b).~~

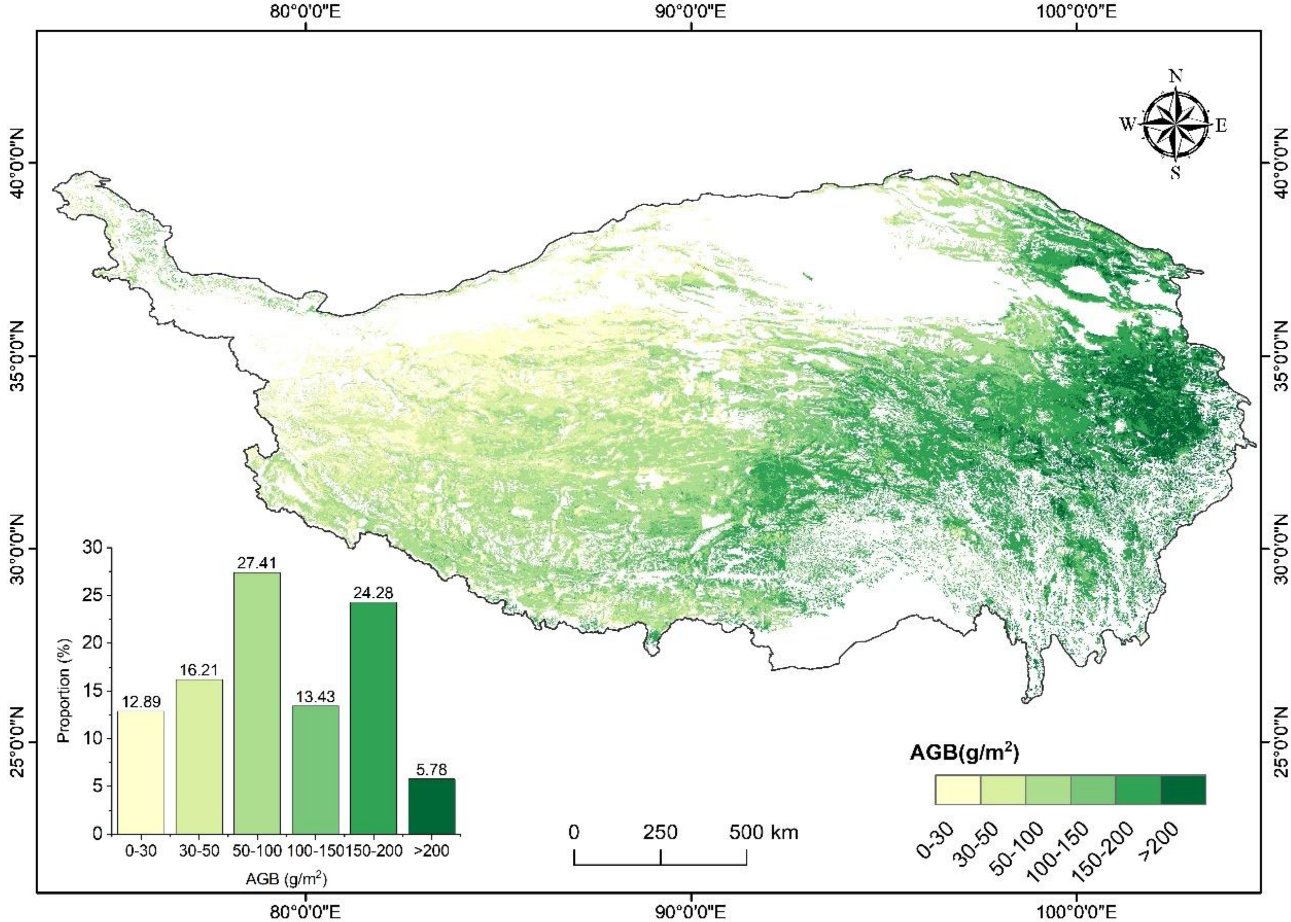

Figure 8.- (a) The spatial distribution of average grassland AGB -on the ~~Qinghai-Tibet Plateau~~QTP ~~during 2000-~~from 2000 to 2019. IID1, IID2, IID3, ID, IIC1, IIC2, IC1, IB1 IIAB1, and OA1 are the eco-geographical regions of the QTP(Zheng, 1996). The full names of each eco-geographical region were listed in Table A5. (b) AGB values of each eco-geographical region from 2000 to 2019. (c) Comparison of multi-year AGB averages in the different eco-geographical regions.

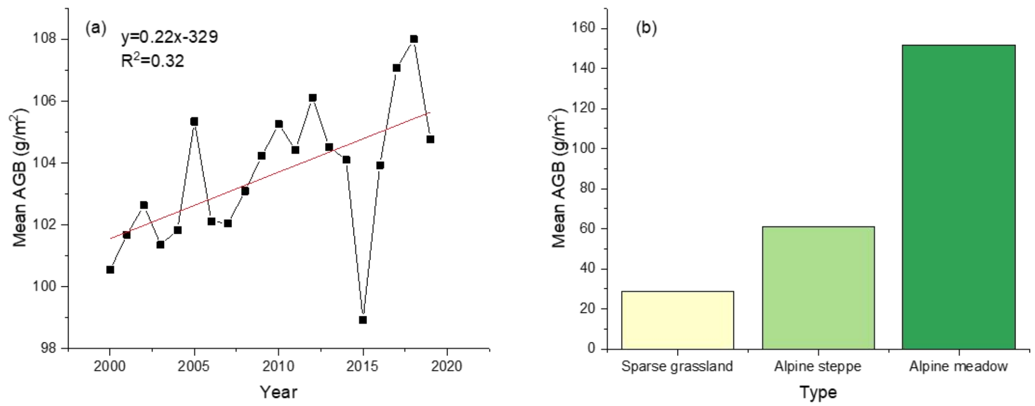

Figure 9. Variation trend of average grassland AGB on the QTP from 2000 to 2019 (a) and average AGB of different grassland types (b).

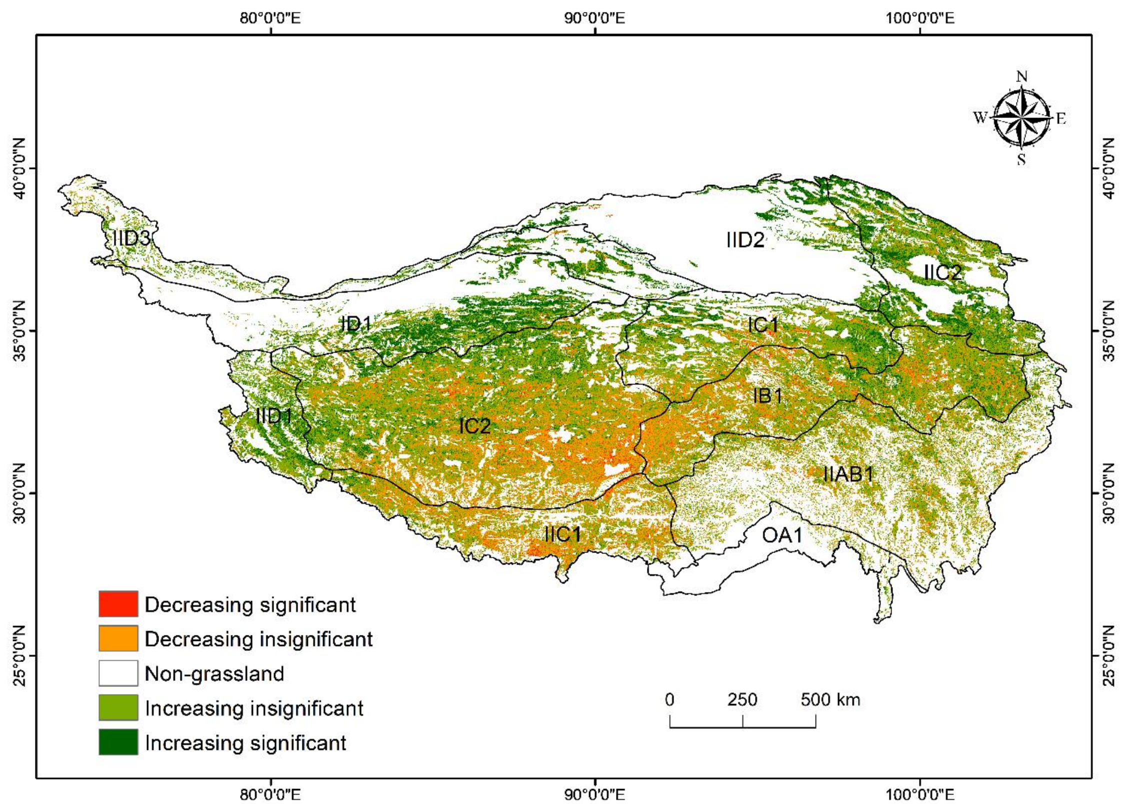

Figure 10. Spatial trends of grassland AGB on the QTP from 2000 to 2019. IID1, IID2, IID3, ID, IIC1, IIC2, IC1, IB1 IIAB1, and OA1 are the eco-geographical regions of the QTP (Zheng, 1996). The full names of each eco-geographical region were listed in Table A5.

4. Discussion

4.1 Scale matching and its influence factor

In ~~Unlike the~~ previous studies, the AGB value of a satellite pixel was ~~directly~~ represented by the average value of 3-5 quadrat-scale samples, so there is a large spatial gap between the ground samples and the satellite pixels ~~-~~(Yang et al., 2017; Yang et al., 2009; Meng et al., 2020)~~, which directly represented the AGB value of a satellite pixel with the average value of 3-5 quadrat-scale samples~~. The spatial gap between ground samples and satellite indices affects the accuracy of grassland AGB models. The smaller the spatial gap between the two, the higher the accuracy of the model (Morais et al., 2021). ~~To address this issue, we used the UAV as a bridge to close the gap~~We addressed this issue using the UAVs as a bridge to reduce the spatial gap~~, this study successfully upscaled the traditional quadrat scale to the MODIS pixel scale~~. ~~We achieved the S~~spatial scale matching of dependent and independent variables was achieved in estimating ~~when calculating the~~ AGB values at different scales. First, at the quadrat scale, the independent variables were all derived from cropped 20-meter-high UAV images corresponding to the ground samples (Figure 3e). Then, the 20-meter-high UAV image was cropped into ~2000 quadrat-sized ~~small~~ patches to ensure consistency with the quadrat~~-~~scale model, and the average of these patches was ~~taken~~ used as the final AGB at the photo~~-~~ scale. Finally, by averaging the AGB of 16 or 12 UAV photos within the MODIS pixel, the AGB ~~AGB~~ value matching ~~that matched~~ the MODIS pixel scale was calculated ~~by the average value ofaveraging the AGB of 16 or 12 UAV photos within the MODIS pixel~~ (Figure A1). ~~Through the above~~ With these three steps, we successfully upscaled the measured AGB from the traditional quadrat scale (0.5 m×0.5 m) to the photo scale (26 m×35 m) and MODIS pixel scale (250 m×250 m). Our results showed that ~~, at the pixel scale,~~ the correlations between the UAV-estimated ~~UAV_estimated~~ AGB values ~~estimated by UAV~~ and the MODIS vegetation ~~indices index~~indices ~~was~~ were higher than that of the traditional sampling method (Figure 7).

Furthermore, we found that the spatial coverage of the UAV sampling had an impact ~~had a particular influence~~ on the ~~the effect s of~~ scale matching. Our results ~~indicated~~ showed that the closer the spatial coverage of the UAV sampling was to the satellite pixel, the higher its correlation with MODIS spectral indices (Figure 7a). ~~This~~It ~~is~~was also confirmed by comparing~~The comparison of~~ the validation results ~~of~~ of different flight modes~~also confirmed this~~. At the pixel scale, we found that the R^2 between the model predictions and the AGB values estimated based on the GRID mode was better than that of RECTANGLE (Figure 11).~~At the pixel scale, we found a higher correlation between the model predictions and the AGB estimates obtained based on the GRID model than the RECTANGLE model (Figure 11).~~ ~~At the pixel scale, we found that UAV AGB estimates from the GRID mode had a higher correlation with the mode predictions than the RECTANGLE flight mode (Figure 10).~~ The reason is that GIRD mode can take 16 pictures within a MODIS pixel, while RECTANGLE mode only takes 12 pictures (Figure A1).~~The reason was that the GIRD mode could obtain 16 photos in the MODIS pixel at a time, while the RECTANGLE mode could only take 12 photos.~~

The above results confirmed that UAV~~s~~s could serve as a bridge to effectively ~~narrow~~ ~~close~~reduce the spatial gap between traditional samples and satellite data.

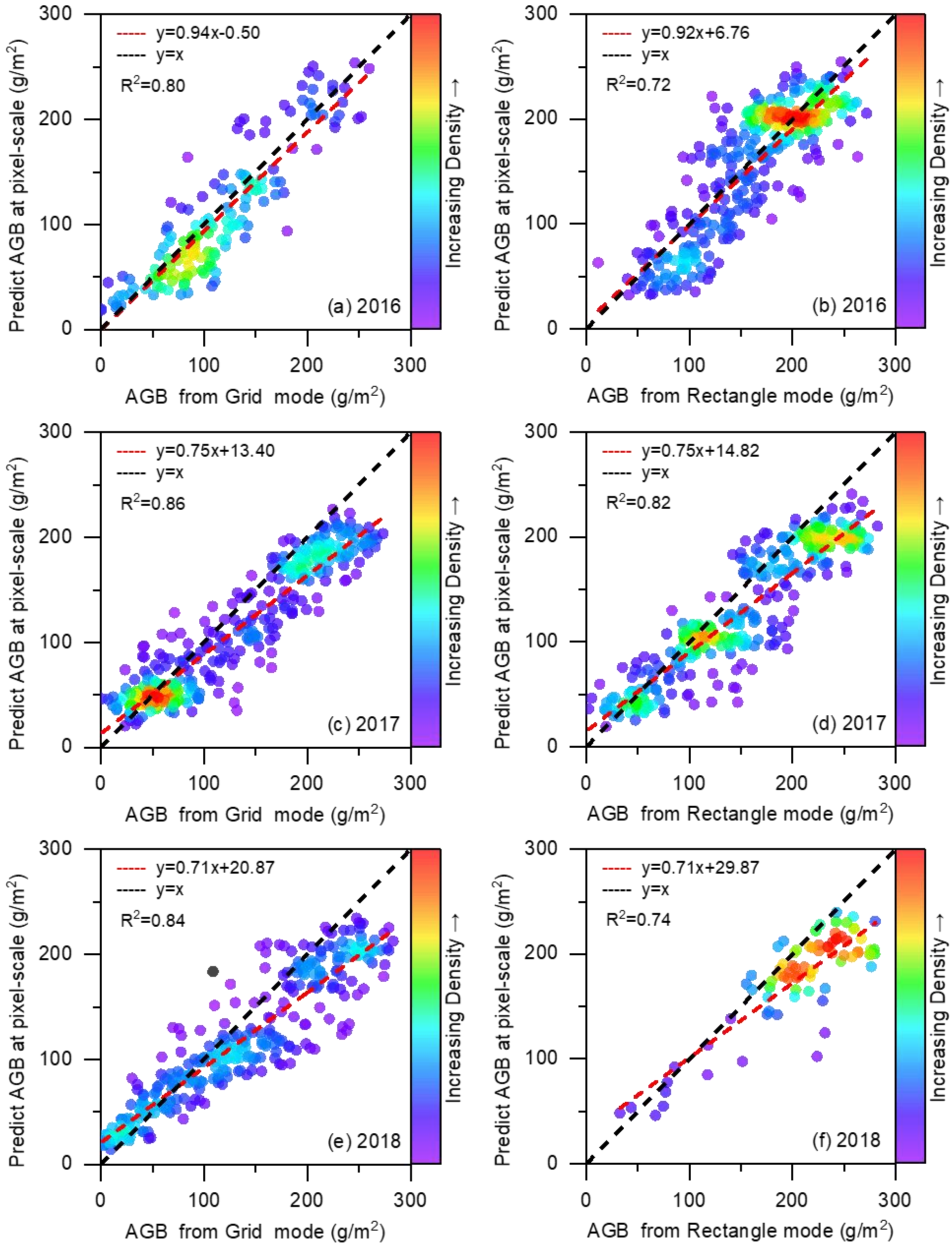
y=0.94x-0.50
y=x
R^2=0.80
(a) 2016
y=0.92x+6.76
y=x
R^2=0.72
(b) 2016
y=0.75x+13.40
y=x
R^2=0.86
(c) 2017
y=0.75x+14.82
y=x
R^2=0.82
(d) 2017
y=0.71x+20.87
y=x
R^2=0.84
(e) 2018
y=0.71x+29.87
y=x
R^2=0.74
(f) 2018
Predict AGB at pixel-scale (g/m^2)
AGB from Grid mode (g/m^2)
AGB from Rectangle mode (g/m^2)
Increasing Density →
0
100
200
300

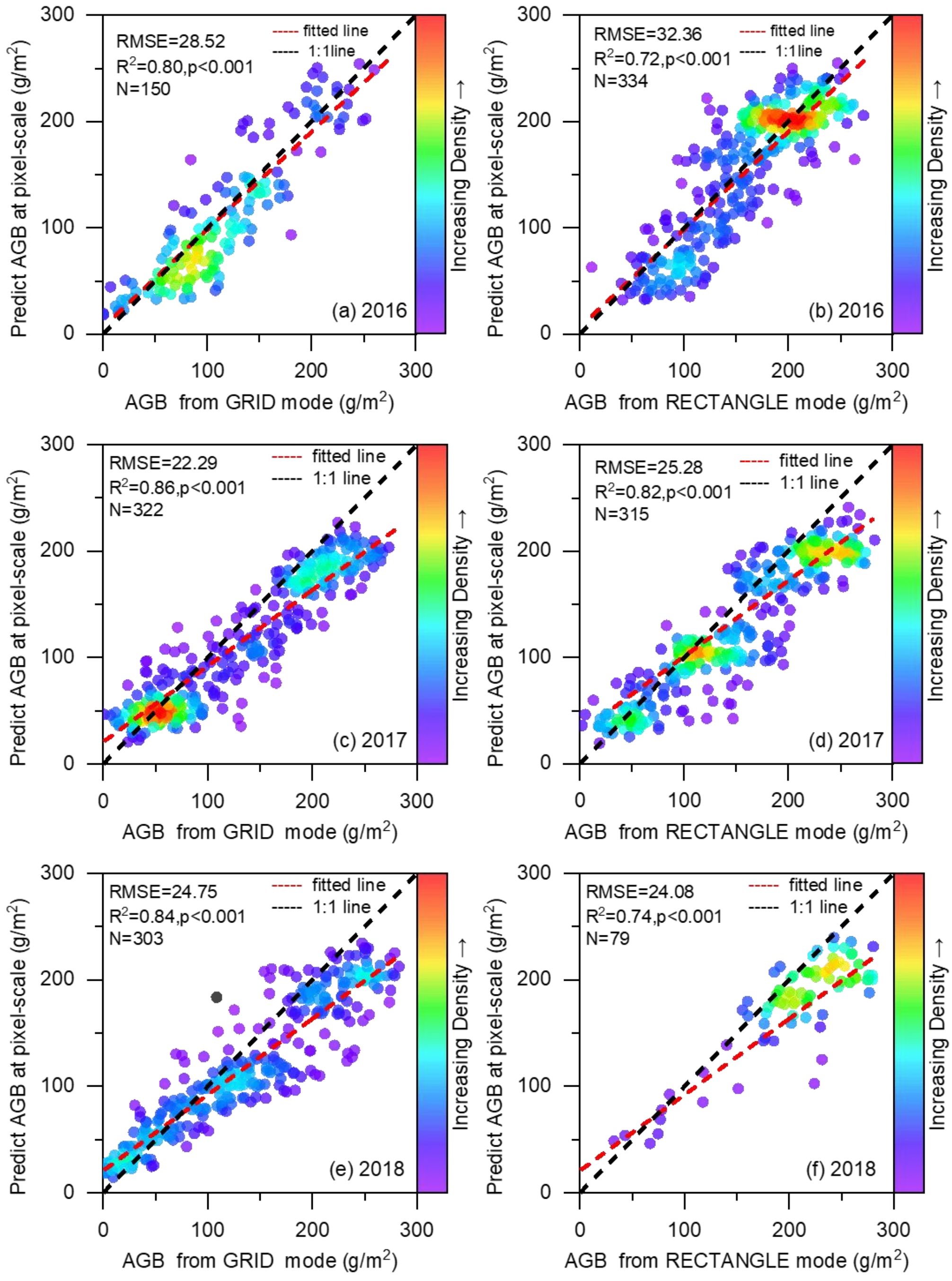

Figure ~~10~~11. Comparison of validation results for the GRID (a,c,e) and RECTANGLE (b,d,f) modes in 2016-2018.

4.2 Importance of the addition of non-vegetation samples

Compared with traditional sampling, UAV sampling has the advantage of wide spatial coverage (0.5 m×0.5 m vs.~~VS~~ 35 m×26 m). Thus, ~~vegetation and non-vegetation background information, such as roads, water, soil, gravel, riverbed, etc., were captured on the UAV photos~~the UAV image could capture vegetation and non-vegetation background information, such as roads, water, soil, gravel, riverbed, etc. (Figure A4~~Figure 11~~12). Adding ~~The addition of~~ non-~~vegetated~~ vegetation samples could improve the ~~estimation~~ accuracy of A~~-A~~GB estimation at the photo scale, especially for low-~~-coverage~~cover areas, ~~,~~ to avoid overestimation. ~~The~~ It ~~same~~ was also true for the pixel-~~-~~scale AGB estimation model. However, the ~~less consideration was given to the non-vegetated areas in the traditional method~~traditional sampling method gave less consideration to the non-vegetation ~~vegetated~~ areas. The sample plots were mainly set ~~-~~in areas with ~~the~~ homogeneous ~~uniform~~ spatial distribution, ~~-~~and rarely ~~but few~~ in areas with spatial heterogeneity. This ~~defect~~ shortcoming ~~might~~ may limit the accuracy of AGB estimation due to the high spatial heterogeneity of the QTP. Fortunately, the UAV sampling method ~~could~~ can avoid this drawback. It can objectively record surface information and reduce the influence of manual plot selection on AGB estimation.~~It could objectively record the ground surface information with both vegetated and non-vegetated areas, resulting in a more objective AGB estimation at the pixel scale.~~

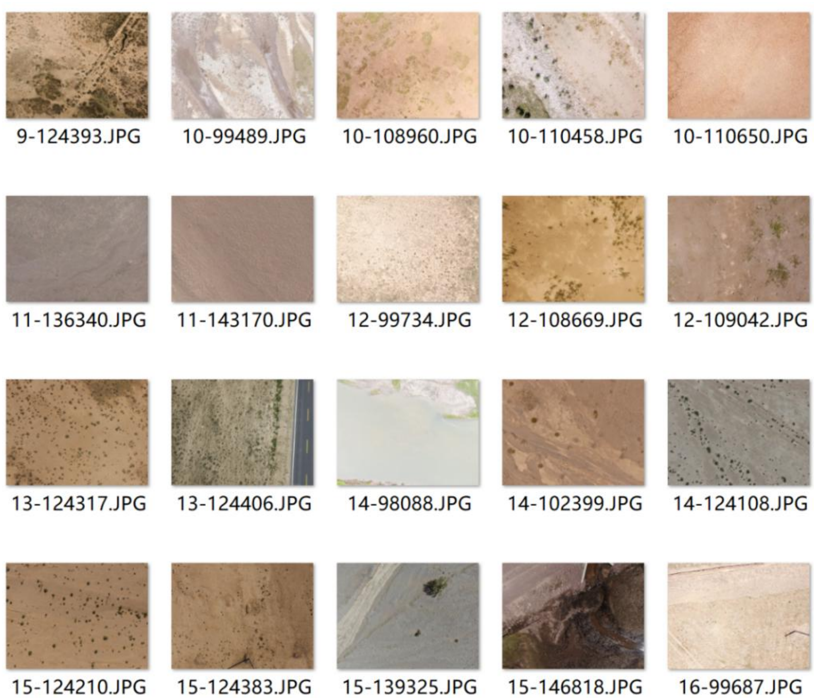

~~**Figure 11**~~**12**~~**. Examples of 20-meter-high UAV images with different non-vegetation background information.**~~

4.3 Comparison of the estimated AGB with previous studies

We compared our results~~In the following, the AGB estimation results of this study were compared~~ with previous studies~~those of others~~ at the quadrat, pixel, and regional scales.~~at the quadrat scale, pixel scale, and regional scale.~~

At the quadrat scale, consistent with our previous study, we further confirmed that the UAV RGB images could be used to estimate grassland AGB ~~at the quadrat scale over a large region~~ (Zhang et al., 2022a; Zhang et al., 2018). Similar to the 2-meter-high UAV image, the indices from the 20-meter-high UAV images could ~~also~~ be used to estimate the grassland AGB at the quadrat-scale (R^2=0.73, RMSE=44.23 g/m^2,~~). The quadrat-scale UAV model had an excellent grassland AGB estimation ability in the range of 0-150 g/m^2, and the verification points were mainly distributed near the 1:1 line~~ (Figure 6a). Compared with the 2-meter-high UAV image, the 20-meter-high UAV image is more suitable for matching the MODIS pixel due to its wider spatial coverage (26 m ×35 m).

At the pixel scale, compared with other studies, this paper achieved the spatial scale matching of independent ~~variables~~ and dependent variables ~~in the~~ during the ~~modeling~~modeling. In previous studies ~~process~~ (Yang et al., 2009; Yang et al., 2017; Meng et al., 2020)~~.~~, they ~~directly~~ constructed the models from the measured AGB values at the quadrat-scale and the spectral indices of the satellites without considering the spatial scale difference. It partly explained~~s~~ why the R^2 of the AGB linear model constructed by Yang et al. was only 0.4 (Yang et al., 2009). Our results ~~also~~ confirmed that ~~after considering the scale difference between measured AGB and NDVI,~~ the R^2 of the linear model could be increased from 0.29 to 0.78 after reducing the spatial gap between measured AGB and NDVI (Figure 7). In addition, thanks to the rapid sampling of UAV AGB, a total of 2,602 samples matching the pixel scale were collected during 2015-2019. It allowed us to perform ~~multi-year~~ cross-year validation to assess the robustness of the model ~~at different times~~over time~~of AGB models at pixel scale to verify the model's robustness in different years~~, which ~~was~~has rarely been performed in previous studies. Our results showed similar validation results for 2017-2019 (R^2=0.85, p<0.001) ~~des~~ despite different sample sizes and spatial distributions (Figure 1, Table 1)~~.~~

~~However, previous studies only randomly selected 20-30% of samples and rarely considered the independence of samples on the time scale.~~

~~In addition, we implemented large-region and multi-year cross-validation in model verification. Despite differences in sample size and spatial distribution (Figure 1, Table 1), the validation results for 2017-2019 were similar (R^2=0.85)~~. But in 2015-2016, R^2 was relatively low, at 0.63 and 0.77, respectively (Table 3, Figure 6). The reason was that during 2015-2016, ~~due to the improper setting, many~~ some photos with abnormal white balance were obtained due to improper settings, which reduced the ~~accuracy of the estimation~~estimation accuracy (Figure A5~~Figure 1213~~). The validation results showed that the pixel-scale AGB estimation model had good robustness in different regions and times when the photo quality was acceptable. ~~The validation results indicated~~ show that ~~that the pixel-~~ ~~scale AGB estimation mode~~ has ~~l had good good~~

~~adaptability robustness in different regions and times when the photo quality is acceptableperiods while obtaining high-quality UAV images. Therefore, this method can be used to estimate the AGB values matching the satellite pixel scale in large regions.~~

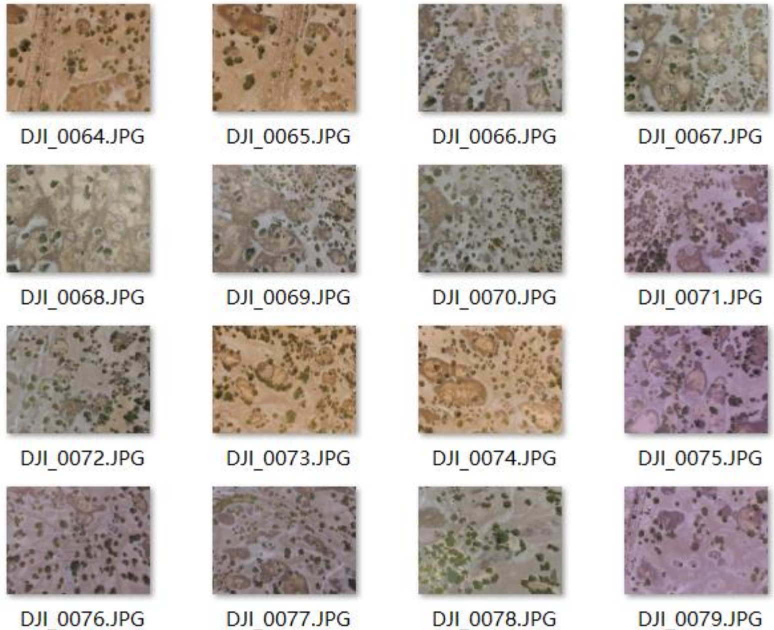

~~**Figure 1213. An example of a set of GIRD photos with abnormal white balance in 2015.**~~

Table ~~4~~5: Comparison of AGB estimation results of different studies on the QTP

Mean AGB (g/m^2)	Alpine steppe (g/m^2)	Alpine meadow (g/m^2)	Study period	Approach	Input parameter ~~Data source~~	References
68.8	50.1	90.8	2001-2004	Linear regression	~~MODIS~~ EVI	(Yang et al., 2009)
__	22.4	42.37	2000-2012	Linear regression	~~MODIS~~ NDVI	(Liu et al., 2017)
120.73	__	__	1980–2014	Exponential regression	NDVI	(Jiao et al., 2017)
78.4	__	__	1982-2010	RF	~~GIMMS~~NDVI, climate	(Xia et al., 2018)
77.12	76.43	154.72	2000-2014	RF	NDVI, EVI, climate, terrain~~MODIS~~	(Zeng et al., 2019)
59.63	42.75	77.56	2000-2017	RF	~~MODIS~~NDVI, climate	(Gao et al., 2020)
~~120.73~~	~~—~~	~~—~~	~~1980–2014~~	~~Regression~~	~~MODIS~~	(Jiao et al., 2017; Zhang et al., 2022b)
102.4	__	__	2000-2020	RF	climate, soil, and	(Zhang et al.,

					terrain	2022b)
70.00	__	__	1960–2002	Century	c~~C~~limate and soil data	(Zhang et al., 2007)
119.78	__	__	2002–2004	Orchidee	c~~C~~limate, soil and LAI data	(Tan et al., 2010)
103.6	60.85	151.85	2000-2019	RF	MODIS	this study

At the regional scale, consistent with previous results, we found an overall increase in AGB over the QTP from 2001 to 2019, albeit with ~~although there were~~ fluctuations ~~among years~~ (Zeng et al., 2019; Gao et al., 2020). The annual average AGB of grassland was 103.6 g/m^2, which was closest to Zhang et al.(Zhang et al., 2022b) and within the range of the previous estimates (59.63-120.73 g/m^2) (Table 5).~~The annual mean AGB of grassland was 103.6 g/m^2, within the previously estimated range (59.63-120.73 g/m^2) (Table 4)~~ ~~.~~The mean AGB varied among ~~of~~ different grassland types~~ was different~~, with 151.85 g/m^2 for~~among which~~ the ~~the~~ alpine meadow ~~was 151.85 g/m^2,~~ and 60.85 g/m^2 for the alpine steppe ~~was 60.85 g/m^2~~. Our estimation results were similar to those of Zeng et al. (Zeng et al., 2019), but the overall average AGB was higher than their estimate~~d~~ of 77.12 g/m^2. ~~-~~The spatial distribution of AGB was consistent with previous studies, showing a west-to-east increasing trend (Zhang et al., 2022b; Xia et al., 2018). Specifically, the average AGB of OA1, IIAB, IB1, and IIC2 eco-geographical regions in the east was significantly higher than that of IID2, IID3, IC2, IID1, and ID1 regions in the west (Figure 8). In general, the average AGB estimates for each eco-geographical region in this paper were not much different from those of Zhang et al. (2022b). Among them, our average AGB estimates for ID1, IID1, IID3, and IID2 regions were slightly lower, but our values were closer to the measured values of these regions (Figure 8c). The reason may be that they calculated the potential ~~biomass~~AGB, while we calculated the actual ~~biomass~~AGB, so our estimate was relatively low.~~The reason may be that they calculate the potential biomass, while we calculate the actual biomass, so the estimate is low.~~ In terms of spatial and temp~~ro~~oral trends, the data results showed that the eco-geographical regions in the northern part of the QTP demonstrated an increasing trend (IID3, ID1, IID2, and IIC2), while the IC2, IIC1, and IB1 regions exhibited significant or non-significant decrease~~s~~, which was consistent with the results of others (Gao et al., 2020; Liu et al., 2017).

The difference between our estimated grassland AGB and previous studies might be due to differences in data sources and modeling methods. Firstly, the sample size and spatial distribution of ground samples were different. The number of ground samples is the most important variable affecting the accuracy of the grassland AGB estimation model (Morais et al., 2021). ~~-~~ Unlike previous studies, we collected ground ~~verification~~ validation data by combining the traditional sampling method and UAVs. The newly proposed method could overcome the shortcomings of traditional samplings (~~, such as the~~ time-consuming and labor-intensive). ~~It no longer took years of work to~~ It no longer takes years to obtain spatially representative, large-scale ground validation data~~Obtaining sufficient sufficient spatially representative ground verification validation data in over a large regionsarea no longer requires years of work~~ (Yang et al., 2017). ~~-~~With UAV sampling, ~~-~~ground observations matching the satellite pixel scale can be obtained in only 15-20 minutes, which is difficult to achieve in traditional surveys. Our new sampling method not only accelerates the sampling speed and increases the sample size, but also improves the spatial match between ground samples and satellite pixels. As a result, our ground validation data is superior to previous studies in terms of quantity and spatial match to the satellite data. Secondly, the ~~predictor~~input ~~variables~~parameters of AGB estimation models were different. Some scholars used only a single vegetation index (NDVI or EVI), while others combined the vegetation index with meteorological, soil, and terrain indices to construct the AGB estimation models (Table 5). In this study, NDVI, kNDVI, EVI, DEM, and PREC were used as the final predictor variables to construct the AGB estimation model at the pixel scale (Table 2). Thirdly, ~~Through UAV sampling, only 15~20 minutes were needed to complete a ground survey in a pixel range of 250 m × 250 m. In addition, it could effectively reduce the spatial gap between ground verification samples and satellite pixels.~~

~~Meanwhile, different~~ modeling ~~approaches~~ methods might also affect the simulation results. As shown in Table 5, the overall AGB averages of the QTP estimated ~~estimated varied considerably~~ based on different methods (~~,~~such as linear or nonlinear regression, machine learning, and ecological process model methods) varied considerably. Yang et al.(2017) found that the model performance of ANN was much better than the linear regression model when using the same dataset to estimate grassland AGB in the Three-River Headwaters Region of China ~~(Yang et al., 2017)~~. Jia et al.(2016) reported that the model forms could bring 13% uncertainty to the AGB estimation.~~n(Jia et al., 2016).~~ Wang et al. compared the RF with the support vector regression (SVR) machine learning algorithm and found that the RF yielded the best performance in grassland biomass estimation (Wang et al., 2017).

4.4 Limitations and further work

We acknowledge that there are some shortcomings in this study. 1) The predicted values of the quadrat-scale model were underestimated when the measured biomass values were greater than 250 g/m^2 (Figure 6). One reason may be that the number of samples greater than 250 g/m^2 was relatively small, accounting for only 5.18 % of ~~the total~~ all samples. Another reason may be that for high biomass grasslands, a single UAV RGB photo can only reflect information such as vegetation cover and greenness, but not height information. This feature is ~~bound to be~~ very unfavorable for estimating AGB in grassland areas with high vegetation coverage and height. Studies have shown that adding vegetation height information can help improve the estimation accuracy of grassland AGB ~~1) The sample size greater than 200 g/m^2 was insufficient at the quadrat scale, leading to underestimation where AGB was high. We will enlarge the sample size to improve the simulation accuracy in future research. 2) Although the grassland height information could help improve the estimation accuracy of grassland AGB, it was still challenging to obtain grassland height information from UAV RGB images in a large area.~~ (Zhang et al., 2022a; Lussem et al., 2019; Viljanen et al., 2018). In future work, a~~A~~n affordable DJI Zensil L1 Lidar UAV will be introduced to invert the height of the grassland~~t grass heights in future work~~. ~~Thus, in the next step, we will consider using the affordable DJI Zensil L1 Lidar UAV to obtain grassland height information to improve the AGB estimation capability.~~ 2) At the pixel scale, limited by the estimation accuracy of AGB from UAV, there was also some underestimation in the high biomass area. Although the MODIS index closest to the sampling time was chosen for the construction/validation of the AGB estimation model, there ~~is~~was still a time difference between the measured samples and the MODIS indices, which ~~may~~might lead to estimation errors. In addition, the NDVI saturation problem was not considered in this study, which might affect the AGB estimation accuracy of QTP (Tucker, 1979a; Gao et al., 2000; Mutanga and Skidmore, 2004; Tucker, 1979b). In the next step, we will continue to collect samples with high biomass and try to correct the NDVI saturation problem to optimize the simulation accuracy of the data set. 3)~~3)~~ During 2015-2016, ~~we~~our study ~~was~~had just ~~beginning~~started, ~~, just started using UAVs to monitor the health of the grassland,~~ and the appropriate ~~suitable~~ camera parameters ~~and methods~~ were still ~~under~~ being ~~exploration~~explored. ~~Therefore~~As a result, some photos with abnormal white balance were obtained, reducing the accuracy of AGB estimation~~reduced the accuracy of AGB estimation~~ at the photo scale (Figure ~~1213~~A5). 4) We ~~only~~ collected grassland AGB only ~~in~~ during the peak ~~season of vegetation growth~~growing season, and ~~whether~~ the applicability of the proposed method ~~applies~~ to other ~~growing~~ growing seasons~~-~~ needs further study~~remains to be further investigated~~. 5) During the modeling process, due to the limited positioning accuracy, only the center points of the flight ~~route~~ path were used to find the ~~matching~~ corresponding MODIS pixels~~ due to the limited positioning accuracy~~. Moreover, although the UAV images ~~from~~ in GRID or RECTANGLE mode ~~could~~ could cover most areas of a MODIS pixel, full pixel coverage ~~was~~ was still not achieved. Therefore, we will gradually ~~scale up~~upscale to MODIS pixels by combining UAVs with Sentinel-2 or Landsat images.

5. Data availability

The dataset is available from the National Tibetan Plateau/Third Pole Environment Data Center (~~at~~https://doi.org/10.11888/Terre.tpdc.272587). The dataset contains 20 years of AGB spatial data of the QTP with a resolution of 250 m and is stored in TIFF format. The name of the file is "AGB_yyyy.tif", where yyyy represents the year. For example, AGB_2000.tif represents this TIFF file describing the alpine grassland AGB condition of QTP in ~~2005~~2000. The data can be readily imported into standard geographical information system software (e.g., ArcGIS) or accessed programmatically (e.g., MATLAB, Python).

6. Conclusion

~~This study~~ In this study, ~~a new~~a new AGB dataset for alpine grasslands on the QTP was calculated based on traditional ground sampling, UAV photography, and MODIS imagery.~~ presents a new gridded dataset of alpine grassland AGB over the QTP based on traditional ground sampling, UAV photographing, and MODIS images.~~ The uniqueness of this dataset is the use of ~~that when obtaining ground verification data, the~~ UAVs ~~is used~~ as a spatial scale~~-~~matching bridge between traditional ~~local measurement~~ samples and satellite pixels. The study confirmed that the UAV images could be used for AGB estimation at the quadrat /pixel scale, with R^2 of 0.73/0.83 and RMSE of 44.23/34.13 g/m^2, respectively. At the pixel scale, the correlation between AGB estimated by UAV and MODIS vegetation index was higher than that of the traditional sampling method (0.88 vs. 0.53~~-~~).~~At the pixel scale, the AGB estimated by UAV was more correlated with the MODIS vegetation indices than the traditional ground sampling method (0.88 VS 0.53), and~~ Moreover, the spatial scale matching of the dependent and the independent variables was achieved during the ~~model~~ modeling~~construction~~. In addition, we performed a ~~an independent~~ cross-year validation of the pixel-scale AGB estimation model to confirm the robustness of the model and the accuracy of this dataset ~~In addition, the constructed pixel scale model has been independently cross-validated over many years (2015-2019), which confirmed the robustness of the model and ensured the accuracy of this dataset~~. ~~Availability~~ The availability of the new dataset is helpful in many applications. First, this dataset provides reliable regional data for estimating grassland productivity, carbon storage, ecological ~~environment~~ carrying capacity, and ecological service functions (such as feed for grazing livestock) ~~on~~of the QTP. Second, the dataset can be used to understand the mechanisms of environmental processes, such as hydrological cycle processes, soil erosion and degradation, and carbon cycle processes in the QTP. In addition, this dataset can be used as input or validation parameters for various ecological models to understand the response mechanism of the QTP to global climate change.

7. Author contributions

HZ contributed to the study conceptualization, methodology, funding acquisition, and the original draft of the manuscript. ZT, BW, and HK contributed to resources and formal analysis. QY and YS contributed to data collection and manuscript review. BM, ML, and JC contributed to the methodology and reviewed the manuscript. YL and JZ participated in reviewing and editing the manuscript. SN contributed to the data collection and review of the manuscript. SY contributed to the study conceptualization, funding acquisition, and manuscript review. All authors~~hip~~ have read and approved the manuscript.

8. Competing interests

The authors declare that they have no conflict of interest.

9. Acknowledgements

We would like to express our gratitude to the other students and staff who participated in the field investigation.

10. Financial support

This research was supported by the National Natural Science Foundation of China [grant nos: 41801023], the National Key R&D Program of China [grant nos: 2017YFA0604801], and the National Natural Science Foundation of China [grant nos: 41801102].

Appendix

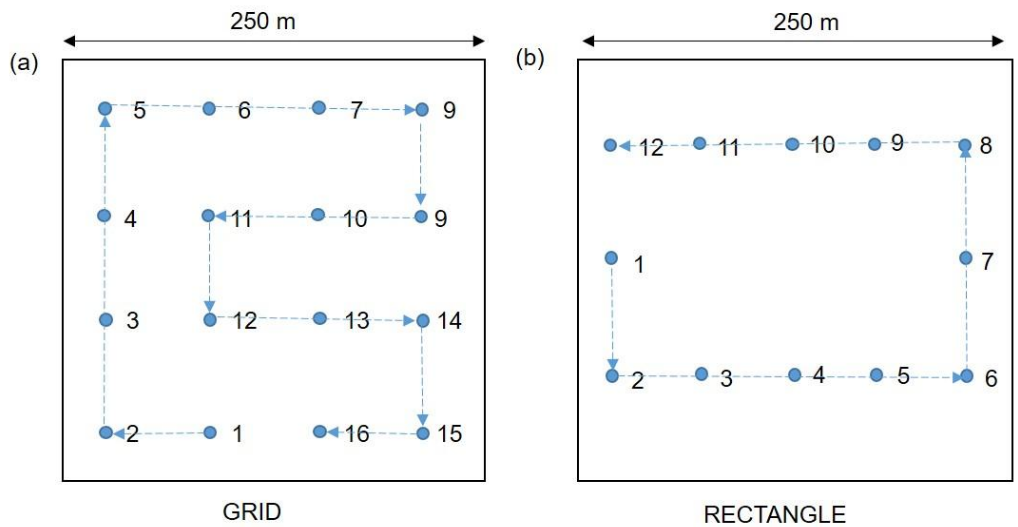

Figure A1. Waypoints for GRID (a) and RECTANGLE (b) flight modes.

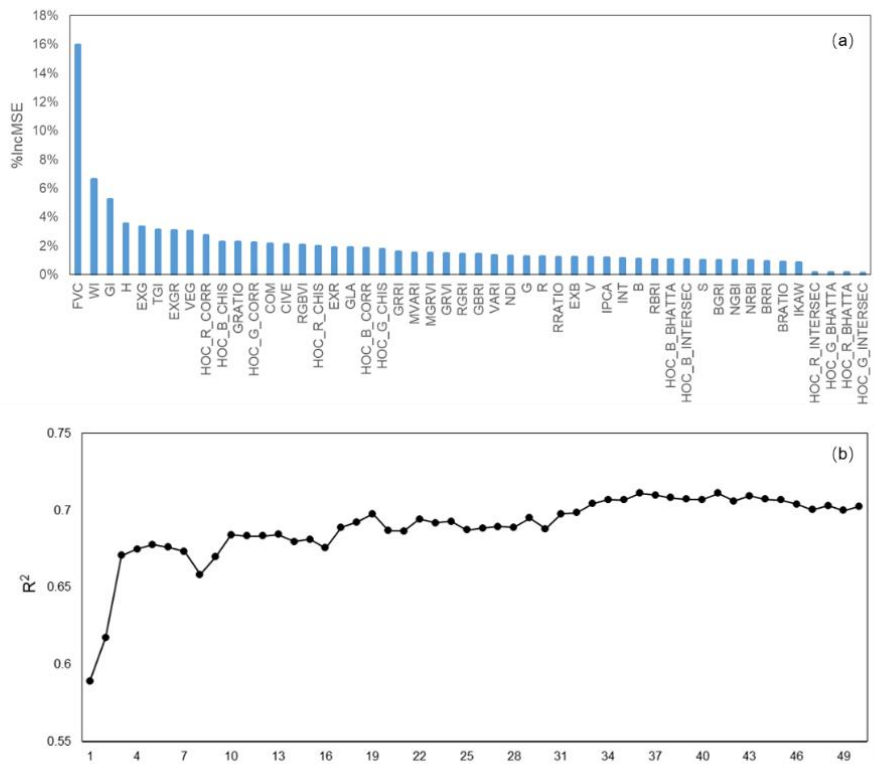

Figure A2. The importance values for each independent variable (a) and the R^2 results of the different number of input variables at the quadrat scale.

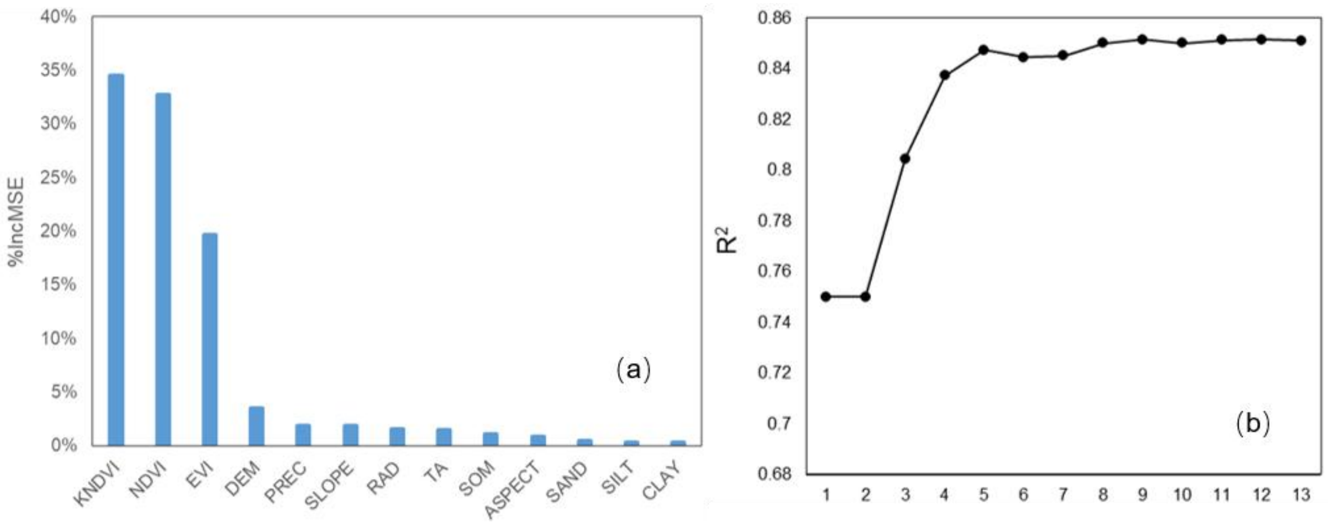

Figure A3. The importance values for each independent variable (a) and the R^2 results of the different number of input variables at the pixel scale.

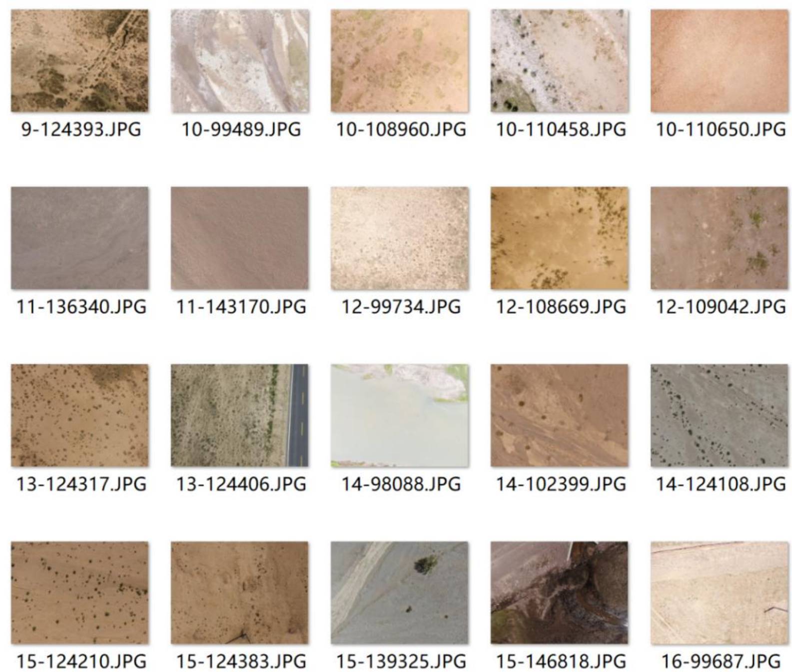

Figure A4. Examples of 20-meter-high UAV images with different non-vegetation background information.

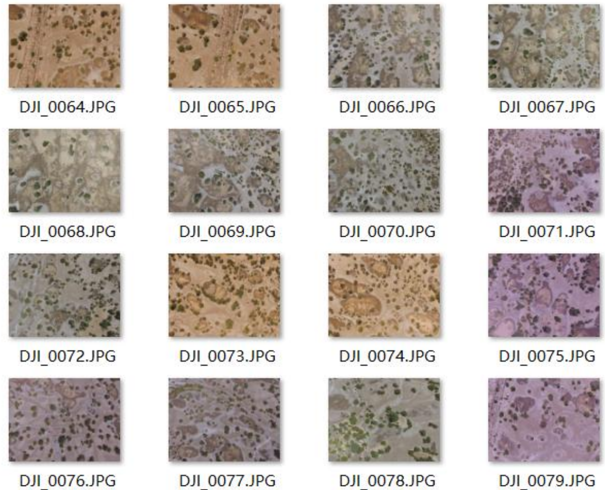

Figure A5. An example of a set of GIRD photos with abnormal white balance in 2015.

Table A1. Combined grassland types

New grassland type	Original grassland type
Alpine meadow	Alpine meadow, Lowland meadow, Montane meadow，
Alpine steppe	Temperate steppe, Alpine steppe, Alpine meadow steppe
Spare grassland	Temperate steppe desert, Alpine desert

Table A2. Features of DJI Phantom 3 Pro

	Features	Description
	Sensor	1/23-inch; Effective-pixel: 12-megapixel
	Filed of view	FOV 94° 20 mm
	Aperture	f/2.8
	Shooting speed	Electronic shutter: 8-1/8000 s
	Photo size	4000×3000
	Flight time	~25 min
DJI Phantom 3 Pro	Image format	JPEG
	Hovering accuracy	±0.5 m vertically; ±1.5 m horizontally
	Weight	1280 g

Table A3: Details of the independent variables for quadrat-scale AGB estimation

Acronym	Index name	Formula	Reference
GRVI	Green Red Vegetation Index	(G-R)/(G+R)	(Tucker, 1979a)
EXG	Excess Green Vegetation Index	2G-R-B	(Woebbecke et al., 1995)
GLA	Green leaf area	(2G-R-B)/(2G+R+B)	(Louhaichi et al.)
MGRVI	Modified Green Blue Vegetation Index	(G2-R2)/(G2+R2)	(Bendig et al., 2015)
RGBVI	Red Green Blue Vegetation Index	(G2-B*R)/(G2+B*R)	(Bendig et al., 2015)
EXB	Excess Blue Vegetation Index	(1.4*B-G)/(G+R+B)	(Maimaitijiang et al., 2019)
NDI	Normalized difference index	(R-G)/(R+G)	(Woebbecke et al., 1993)
EXR	Excess Red Vegetation Index	1.4*R-B	(Meyer and Neto, 2008)
EXGR	Excess Green minus Excess Red index	ExG−ExR	(Meyer and Neto, 2008)
RRATIO	Red Ratio	R/(R+B+G)	(Woebbecke et al., 1995)
BRATIO	Blue Ratio	B/(R+B+G)	(Woebbecke et al., 1995)
GRATIO	Green Ratio	G/(R+B+G)	(Woebbecke et al., 1995)
VARI	Visible Atmospherically Resistance Index	(G -R)/(G + R - B)	(Gitelson et al., 2002)
NRBI	Normalized Red Blue Index	(R-B)/(R+B)	(Michez et al., 2016)
NGBI	Normalized Green Blue Index	(G-B)/(G+B)	(Michez et al., 2016)
VEG	Vegetative index	G/(RaB(1-a)),where a=0.667	(Hague et al., 2006)
WI	Woebbecke Index	(G−B)/(R−G)	(Woebbecke et al., 1995)
CIVE	Color Index of Vegetation	0.441R – 0.881G+0.385B+18.78745	(Kataoka et al., 2003)
COM	Combination Vegetative index	0.25ExG+0.3ExGR+0.33CIVE +0.12VEG	(Guijarro et al., 2011)
TGI	Triangular Greenness Index	G-0.39R-0.61B	(Hunt et al., 2014; Michez et al., 2018)
RGBVI	Red Green Blue Vegetation Index	(G2-B*R)/(G2+B*R)	(Bendig et al., 2015)
GRRI	Green Red Ratio Index	G/R	(Maimaitijiang et al., 2019)
GBRI	Green Blue Ratio Index	G/B	(Maimaitijiang et al., 2019)
RBRI	Red Blue Ratio Index	R/B	(Maimaitijiang et al., 2019)
BRRI	Blue Red Ratio Index	B/R	(Jibo et al., 2018)
BGRI	Blue Green Ratio Index	B/G	(Jibo et al., 2018)
RGRI	Red Green Ratio Index	R/G	(Jibo et al., 2018)
INT	Color Intensity Index	(R+B+G)/3	(Ahmad and Reid, 1996)
MVARI	Modified VARI	(G-B)/(G+R-B)	(Cen et al., 2019)
IPCA	Principal Component Analysis Index	$0.994\times\lvert R-B\rvert + 0.961\times\lvert G-B\rvert + 0.914\times\lvert G-R\rvert$	(Saberioon et al., 2014)

Table A3: Details of the independent variables for quadrat-scale AGB estimation (continued)

Acronym	Index name	Formula	Reference
R	An average value of R channel of the quadrat-scale UAV image		
G	An average value of G channel of the quadrat-scale UAV image		
B	An average value of B channel of the quadrat-scale UAV image		
H	An average value of H channel of the quadrat-scale image in HSV color space		
S	An average value of S channel of the quadrat-scale image in HSV color space		
V	An average value of V channel of the quadrat-scale image in HSV color space		
FVC	Fractional Vegetion Cover		
EGI	Extra Geen Index	EGI=2G-R-B	
GI	Green Index	GI=9×(H×3.14159/180) +3×S+V	(Zhang et al., 2022a)
HOC_*i*_CORR	The histogram correlation coefficient between the *i* band and the black reference histogram, where the *i* represents the three bands of RGB	$corr\frac{\sum_I (H_1(I)-\bar{H}_1)(H_2(I)-\bar{H}_2)}{\sqrt{\sum_I (H_1(I)-\bar{H}_1)^2 \sum_I (H_2(I)-\bar{H}_2)^2}}$	
HOC_*i*_INTERSEC	The histogram intersection coefficient between the *i* band and the black reference histogram, where the *i* represents the three bands of RGB	$intersec = \sum_I \min(H_1(I), H_2(I))$	
HOC_*i*_BHATTA	The histogram Bhattacharyya distance coefficient between the *i* band and the black reference histogram, where the *i* represents the three bands of RGB	$bhatta = \sum_I \min(H_1(I), H_2(I))$	
HOC_*i*_CHIS	The histogram correlation coefficient between the *i* band and the black reference histogram, where the *i* represents the three bands of RGB.	$chis = \sum_I \frac{\left(H_1(I)-H_2(I)\right)^2}{H_1(I)}$	

Table A4：Regression analysis for AGB estimation models at quadrat and pixel scales~~Statistical information of regression models for AGB estimation models at quadrat and pixel scales~~

Model name	Coefficient	Value	Standard Error	t-Value	p-value
2019_Quadrat-scale	Slope	0.67	0.016	42.58	9.05e-194
	Intercept	20.10	1.49	13.59	5.96e-37
2019_Pixel_scale	Slope	0.84	0.03	31.59	2.75e-73
	Intercept	23.20	4.04	5.74	4.24e-8
2018_Pixel_scale	Slope	0.73	0.02	45.81	8.28e-157
	Intercept	20.43	2.74	7.46	6.01e-13
2017_Pixel_scale	Slope	0.75	0.01	59.13	1.98e-260
	Intercept	13.89	2.04	6.82	2.19e-11
2016_Pixel_scale	Slope	0.94	0.02	40.45	4.69e-157
	Intercept	2.48	3.75	0.66	0.03
2015_Pixel_scale	Slope	0.82	0.04	18.88	2.59e-47
	Intercept	9.50	5.25	1.81	0.04

Table A5: List of abbreviations of eco-geographical regions and the mean AGB of the QTP

Abbreviation	Full name
IB1	Golog-Nagqu high-cold shrub-meadow zone
IIAB1	Western Sichuan-eastern Tibet montane coniferous forest zone
IC1	Southern Qinghai high-cold meadow steppe zone
IC2	Qiangtang high-cold steppe zone
ID1	Kunlun high-cold desert zone
IIC1	Southern Tibet montane shrub-steppe zone
IIC2	Eastern Qinghai-Qilian montane steppe zone
IID1	Nagri montane desert-steppe and desert zone
IID2	Qaidam montane desert zone
IID3	Northern slopes of Kunlun montane desert zone
OA1	Southern slopes of Himalaya montane evergreen broad-leaved forest zone

References

Ahmad, I. S. and Reid, J. F.: Evaluation of Colour Representations for Maize Images, Journal of Agricultural Engineering Research, 63, 185-195, doi:10.1006/jaer.1996.0020 1996.4

Bendig, J., Yu, K., Aasen, H., Bolten, A., Bennertz, S., Broscheit, J., Gnyp, M. L., and Bareth, G.: Combining UAV-based plant height from crop surface models, visible, and near infrared vegetation indices for biomass monitoring in barley, International Journal of Applied Earth Observation & Geoinformation, 39, 79-87, doi:10.1016/j.jag.2015.02.012, 2015.4

Bian, L. and Walsh, S. J.: Scale dependencies of vegetation and topography in a mountainous environment of Montana, The Professional Geographer, 45, 1-11, doi:10.1111/j.0033-0124.1993.00001.x, 1993.4

Breiman, L.: Random forests, Machine learning, 45, 5-32, doi:10.1023/A:1010933404324, 2001.4

Camps-Valls, G., Campos-Taberner, M., Moreno-Martinez, A., Walther, S., Duveiller, G., Cescatti, A., Mahecha, M. D., Munoz-Mari, J., Garcia-Haro, F. J., Guanter, L., Jung, M., Gamon, J. A., Reichstein, M., and Running, S. W.: A unified vegetation index for quantifying the terrestrial biosphere, Sci Adv, 7, eabc7447, doi:10.1126/sciadv.abc7447, 2021.4

Cannavacciuolo, M., Bellido, A., Cluzeau, D., Gascuel, C., and Trehen, P.: A geostatistical approach to the study of earthworm distribution in grassland, Applied Soil Ecology, 9, 345-349, doi:10.1016/S0929-1393(98)00087-0, 1998.4

Cen, H. Y., Wan, L., Zhu, J. P., Li, Y. J., Li, X. R., Zhu, Y. M., Weng, H. Y., Wu, W. K., Yin, W. X., Xu, C., Bao, Y. D., Feng, L., Shou, J. Y., and He, Y.: Dynamic monitoring of biomass of rice under different nitrogen treatments using a lightweight UAV with dual image-frame snapshot cameras, Plant Methods, 15, doi:10.1186/s13007-019-0418-8, 2019.4

Chen, J., Yi, S., Qin, Y., and Wang, X.: Improving estimates of fractional vegetation cover based on UAV in alpine grassland on the Qinghai–Tibetan Plateau, International Journal of Remote Sensing, 37, 1922-1936, doi:10.1080/01431161.2016.1165884, 2016.4

Cheng, X., An, S., Chen, J., Li, B., Liu, Y., and Liu, S.: Spatial relationships among species, above-ground biomass, N, and P in degraded grasslands in Ordos Plateau, northwestern China, Journal of Arid Environments, 68, 652-667, doi:10.1016/j.jaridenv.2006.07.006, 2007.4

Crow, W. T., Berg, A. A., Cosh, M. H., Loew, A., Mohanty, B. P., Panciera, R., de Rosnay, P., Ryu, D., and Walker, J. P.: Upscaling sparse ground - based soil moisture observations for the validation of coarse - resolution satellite soil moisture products, Reviews of Geophysics, 50, doi:10.1029/2011rg000372, 2012.4

Dancy, K., Webster, R., and Abel, N.: Estimating and mapping grass cover and biomass from low-level photographic sampling, International Journal of Remote Sensing, 7, 1679-1704, doi:10.1080/01431168608948961, 1986.4

Ding, M. J., Zhang, Y. L., Sun, X. M., Liu, L. S., Wang, Z. F., and Bai, W. Q.: Spatiotemporal variation in alpine grassland phenology in the Qinghai-Tibetan Plateau from 1999 to 2009, Chinese Science Bulletin, 58, 396-405, doi:10.1007/s11434-012-5407-5, 2013.4

Dusseux, P., Hubert-Moy, L., Corpetti, T., and Vertes, F.: Evaluation of SPOT imagery for the estimation of grassland biomass, International Journal of Applied Earth Observation and Geoinformation, 38, 72-77, doi:10.1016/j.jag.2014.12.003, 2015.4

Fensholt, R., Rasmussen, K., Nielsen, T. T., and Mbow, C.: Evaluation of earth observation based long term vegetation trends—Intercomparing NDVI time series trend analysis consistency of Sahel from AVHRR GIMMS, Terra MODIS and SPOT VGT data, Remote sensing of environment, 113, 1886-1898, 2009.4

Gao, X., Huete, A. R., Ni, W., and Miura, T.: Optical–biophysical relationships of vegetation spectra without background contamination, Remote sensing of environment, 74, 609-620, 2000.4

Gao, X. X., Dong, S. K., Li, S., Xu, Y. D., Liu, S. L., Zhao, H. D., Yeomans, J., Li, Y., Shen, H., Wu, S. N., and Zhi, Y. L.: Using the random forest model and validated MODIS with the field spectrometer measurement promote the accuracy of estimating aboveground biomass and coverage of alpine grasslands on the Qinghai-Tibetan Plateau, Ecological Indicators, 112, 106114, doi:10.1016/j.ecolind.2020.106114, 2020.4

Ghosh, S. M. and Behera, M. D.: Aboveground biomass estimation using multi-sensor data synergy and machine learning algorithms in a dense tropical forest, Applied Geography, 96, 29-40, doi:10.1016/j.apgeog.2018.05.011, 2018.4

Gitelson, A. A., Kaufman, Y. J., Stark, R., and Rundquist, D.: Novel algorithms for remote estimation of vegetation fraction, Remote Sensing of Environment, 80, 76-87, doi:10.1016/s0034-4257(01)00289-9 2002.4

Guijarro, M., Pajares, G., Riomoros, I., Herrera, P. J., Burgos-Artizzu, X. P., and Ribeiro, A.: Automatic segmentation of relevant textures in agricultural images, Computers & Electronics in Agriculture, 75, 75-83, doi:10.1016/j.compag.2010.09.013, 2011.4

Hague, T., Tillett, N. D., and Wheeler, H.: Automated Crop and Weed Monitoring in Widely Spaced Cereals, Precision Agriculture, 7, 21-32, doi:10.1007/s11119-005-6787-1, 2006.4

He, L., Li, A. N., Yin, G. F., Nan, X., and Bian, J. H.: Retrieval of Grassland Aboveground Biomass through Inversion of the PROSAIL Model with MODIS Imagery, Remote Sensing, 11, 1597, doi:10.3390/rs11131597, 2019.4

Hoaglin, D. C., Mosteller, F., and Tukey, J. W.: Understanding robust and exploratory data anlysis, Wiley series in probability and mathematical statistics, 1983.4

Holben, B. N.: Characteristics of maximum-value composite images from temporal AVHRR data, International journal of remote sensing, 7, 1417-1434, 1986.4

Hunt, E. R., Daughtry, C. S. T., Mirsky, S. B., and Hively, W. D.: Remote Sensing With Simulated Unmanned Aircraft Imagery for Precision Agriculture Applications, IEEE Journal of Selected Topics in Applied Earth Observations & Remote Sensing, 7, 4566-4571, doi:doi:10.1109/jstars.2014.2317876, 2014.4

Jia, W., Liu, M., Yang, Y., He, H., Zhu, X., Yang, F., Yin, C., and Xiang, W.: Estimation and uncertainty analyses of grassland biomass in Northern China: Comparison of multiple remote sensing data sources and modeling approaches, Ecological indicators, 60, 1031-1040, doi:10.1016/j.ecolind.2015.09.001, 2016.4

Jiang, W., Yuan, L., Wang, W., Cao, R., Zhang, Y., and Shen, W.: Spatio-temporal analysis of vegetation variation in the Yellow River Basin, Ecological Indicators, 51, 117-126, 2015.4

Jiao, C., Yu, G., He, N., Ma, A., and Hu, Z.: The spatial pattern of grassland aboveground biomass and its environmental controls in the Eurasian steppe, doi:10.11821/dlxb201605007, 2017.4

Jibo, Y., Haikuan, F., Xiuliang, J., Huanhuan, Y., Zhenhai, L., Chengquan, Z., Guijun, Y., and Qingjiu, T.: A Comparison of Crop Parameters Estimation Using Images from UAV-Mounted Snapshot Hyperspectral Sensor and High-Definition Digital Camera, Remote Sensing, 10, 1138-, doi:10.3390/rs10071138, 2018.4

Kataoka, T., Kaneko, T., Okamoto, H., and Hata, S.: Crop growth estimation system using machine vision, Advanced Intelligent Mechatronics, 2003. AIM 2003. Proceedings. 2003 IEEE/ASME International Conference on, Crop growth estimation system using machine vision,

Kohavi, R.: A study of cross-validation and bootstrap for accuracy estimation and model selection, Ijcai, 1137-1145, doi:10.1109/jstars.2014.2317876,

Li, M., Wu, J., Feng, Y., Niu, B., He, Y., and Zhang, X.: Climate variability rather than livestock grazing dominates changes in alpine grassland productivity across Tibet, Frontiers in Ecology and Evolution, 9, doi:10.3389/fevo.2021.631024, 2021.4

Li, X., Liu, S., Li, H., Ma, Y., Wang, J., Zhang, Y., Xu, Z., Xu, T., Song, L., and Yang, X.: Intercomparison of six upscaling evapotranspiration methods: From site to the satellite pixel, Journal of Geophysical Research: Atmospheres, 123, 6777-6803, doi:10.1029/2018jd028422, 2018.4

Liu, S., Cheng, F., Dong, S., Zhao, H., Hou, X., and Wu, X.: Spatiotemporal dynamics of grassland aboveground biomass on the Qinghai-Tibet Plateau based on validated MODIS NDVI, Scientific reports, 7, 1-10, doi:10.1038/s41598-017-04038-4, 2017.4

Louhaichi, M., Borman, M. M., and Johnson, D.: Spatially Located Platform and Aerial Photography for Documentation of Grazing Impacts on Wheat, Geocarto International, doi:10.1080/10106040108542184,

Lussem, U., Bolten, A., Menne, J., Gnyp, M. L., Schellberg, J., and Bareth, G.: Estimating biomass in temperate grassland with high resolution canopy surface models from UAV-based RGB images and vegetation indices, Journal of Applied Remote Sensing, 13, 034525, doi:10.1117/1.Jrs.13.034525, 2019.4

Maimaitijiang, M., Sagan, V., Sidike, P., Maimaitiyiming, M., Hartling, S., Peterson, K. T., Maw, M. J. W., Shakoor, N., Mockler, T., and Fritschi, F. B.: Vegetation Index Weighted Canopy Volume Model (CVM VI) for soybean biomass estimation from Unmanned Aerial System-based RGB imagery, ISPRS Journal of Photogrammetry and Remote Sensing, 151, 27-41, doi:10.1016/j.isprsjprs.2019.03.003, 2019.4

Meng, B., Yi, S., Liang, T., Yin, J., and Sun, Y.: Modeling alpine grassland above ground biomass based on remote sensing data and machine learning algorithm: A case study in the east of Tibetan Plateau, China, IEEE Journal of Selected Topics in Applied Earth Observations and Remote Sensing, PP, 1-1, doi:10.1109/Jstars.2020.2999348, 2020.4

Meyer, G. E. and Neto, J. C.: Verification of color vegetation indices for automated crop imaging applications, Computers and Electronics in Agriculture, 63, 282-293, doi:10.1016/j.compag.2008.03.009, 2008.4

Michez, A., Piégay, H., Lisein, J., Claessens, H., and Lejeune, P.: Classification of riparian forest species and health condition using multi-temporal and hyperspatial imagery from unmanned aerial system, Environmental Monitoring & Assessment, 188, 1-19, doi:10.1007/s10661-015-4996-2, 2016.4

Michez, A., Bauwens, S., Brostaux, Y., Hiel, M. P., Garré, S., Lejeune, P., and Dumont, B.: How Far Can Consumer-Grade UAV RGB Imagery Describe Crop Production? A 3D and Multitemporal Modeling Approach Applied to Zea mays, Remote Sensing, 10, doi:10.3390/rs10111798, 2018.4

Morais, T. G., Teixeira, R. F., Figueiredo, M., and Domingos, T.: The use of machine learning methods to estimate aboveground biomass of grasslands: A review, Ecological Indicators, 130, 108081, doi:10.1016/j.ecolind.2021.108081, 2021.4

Mutanga, O. and Skidmore, A. K.: Narrow band vegetation indices overcome the saturation problem in biomass estimation, International journal of remote sensing, 25, 3999-4014, 2004.4

Mutanga, O., Adam, E., and Cho, M. A.: High density biomass estimation for wetland vegetation using WorldView-2 imagery and random forest regression algorithm, International Journal of Applied Earth Observation and Geoinformation, 18, 399-406, doi:10.1016/j.jag.2012.03.012, 2012.4

O'Mara, F. P.: The role of grasslands in food security and climate change, Annals of botany, 110, 1263-1270, doi:10.1093/aob/mcs209, 2012.4

Ramankutty, N., Evan, A. T., Monfreda, C., and Foley, J. A.: Farming the planet: 1. Geographic distribution of global agricultural lands in the year 2000, Global biogeochemical cycles, 22, doi:10.1029/2007GB002952, 2008.4

Saberioon, M. M., Amin, M., Anuar, A. R., Gholizadeh, A., Wayayok, A., and Khairunniza-Bejo, S.: Assessment of rice leaf chlorophyll content using visible bands at different growth stages at both the leaf and canopy scale, International Journal of Applied Earth Observations & Geoinformation, 32, 35-45, doi:10.1016/j.jag.2014.03.018, 2014.4

Suttie, J. M., Reynolds, S. G., and Batello, C.: Grasslands of the World, Food & Agriculture Org.2005.

Tan, K., Ciais, P., Piao, S., Wu, X., Tang, Y., Vuichard, N., Liang, S., and Fang, J.: Application of theORCHIDEE global vegetationmodel to evaluate biomass and soil carbon stocks ofQinghai-Tibetan grasslands, 2010.4

Tucker, C. J.: Red and photographic infrared linear combinations for monitoring vegetation, Remote Sensing and Environment, 8, 127-150, doi:10.1016/0034-4257(79)90013-0, 1979a.4

Tucker, C. J.: Red and photographic infrared linear combinations for monitoring vegetation, Remote sensing of Environment, 8, 127-150, 1979b.4

Vergara, J. R. and Estévez, P. A.: A review of feature selection methods based on mutual information, Neural computing and applications, 24, 175-186, doi:10.1007/s00521-013-1368-0, 2014.4

Viljanen, N., Honkavaara, E., Näsi, R., Hakala, T., Niemeläinen, O., and Kaivosoja, J.: A novel machine learning method for estimating biomass of grass swards using a photogrammetric canopy height model, images and vegetation indices captured by a drone, Agriculture, 8, 70, doi:10.3390/agriculture8050070, 2018.4

Wang, J. and Sun, W.: Multiscale geostatistical analysis of sampled above-ground biomass and vegetation index products from HJ-1A/B, Landsat, and MODIS, Land Surface Remote Sensing II, 92601T, 10.1117/12.2069008,

Wang, J., Ge, Y., Song, Y., and Li, X.: A geostatistical approach to upscale soil moisture with unequal precision observations, IEEE Geoscience and Remote Sensing Letters, 11, 2125-2129, doi:10.1109/Lgrs.2014.2321429, 2014.4

Wang, J., Xiao, X., Bajgain, R., Starks, P., Steiner, J., Doughty, R. B., and Chang, Q.: Estimating leaf area index and aboveground biomass of grazing pastures using Sentinel-1, Sentinel-2 and Landsat images, ISPRS Journal of Photogrammetry and Remote Sensing, 154, 189-201, doi:10.1016/j.isprsjprs.2019.06.007, 2019.4

Wang, L. a., Zhou, X., Zhu, X., Dong, Z., and Guo, W.: Estimation of biomass in wheat using random forest regression algorithm and remote sensing data, The Crop Journal, 4, 212-219, doi:10.1016/j.cj.2016.01.008, 2016.4

Wang, Y., Shen, X., Jiang, M., Tong, S., and Lu, X.: Spatiotemporal change of aboveground biomass and its response to climate change in marshes of the Tibetan Plateau, International Journal of Applied Earth Observation and Geoinformation, 102, 102385, 2021.4

Wang, Y., Wu, G., Deng, L., Tang, Z., Wang, K., Sun, W., and Shangguan, Z.: Prediction of aboveground grassland biomass on the Loess Plateau, China, using a random forest algorithm, Scientific reports, 7, 1-10, doi:10.1038/s41598-017-07197-6, 2017.4

Woebbecke, D. M., Meyer, G. E., Bargen, K. V., and Mortensen, D. A.: Color Indices for Weed Identification Under Various Soil, Residue, and Lighting Conditions, Transactions of the Asae, 38, 259-269, doi:10.1109/jstars.2014.2317876 1995.4

Woebbecke, D. M., Meyer, G. E., Von Bargen, K., and Mortensen, D. A.: Plant species identification, size, and enumeration using machine vision techniques on near-binary images, Optics in Agriculture and Forestry, 208-219, 10.1117/12.144030

Xia, J., Ma, M., Liang, T., Wu, C., Yang, Y., Zhang, L., Zhang, Y., and Yuan, W.: Estimates of grassland biomass and turnover time on the Tibetan Plateau, Environmental Research Letters, 13, 014020, doi:10.1088/1748-9326/aa9997, 2018.4

Yang, S., Feng, Q., Liang, T., Liu, B., Zhang, W., and Xie, H.: Modeling grassland above-ground biomass based on artificial neural network and remote sensing in the Three-River Headwaters Region, Remote Sensing of Environment, S0034425717304741, doi:10.1016/j.rse.2017.10.011, 2017.4

Yang, Y., Fang, J., Pan, Y., and Ji, C.: Aboveground biomass in Tibetan grasslands, Journal of Arid Environments, 73, 91-95, doi:10.1016/j.jaridenv.2008.09.027, 2009.4

Yang, Y., Fang, J., Ma, W., Guo, D., and Mohammat, A.: Large‐scale pattern of biomass partitioning across China's grasslands, Global Ecology and Biogeography, 19, 268-277, doi:10.1111/j.1466-8238.2009.00502.x, 2010.4

Yi, S.: FragMAP: a tool for long-term and cooperative monitoring and analysis of small-scale habitat fragmentation using an unmanned aerial vehicle, International Journal of Remote Sensing, 38, 2686-2697, doi:10.1080/01431161.2016.1253898, 2017.4

Yu, R., Yao, Y., Wang, Q., Wan, H., Xie, Z., Tang, W., Zhang, Z., Yang, J., Shang, K., and Guo, X.: Satellite-Derived Estimation of Grassland Aboveground Biomass in the Three-River Headwaters Region of China during 1982–2018, Remote Sensing, 13, 2993, doi:10.3390/rs13152993, 2021.4

Zeng, N., Ren, X., He, H., Zhang, L., Zhao, D., Ge, R., Li, P., and Niu, Z.: Estimating grassland aboveground biomass on the Tibetan Plateau using a random forest algorithm, Ecological Indicators, 102, 479-487, doi:10.1016/j.ecolind.2019.02.023, 2019.4

Zhang, B., Zhang, L., Xie, D., Yin, X., Liu, C., and Liu, G.: Application of synthetic NDVI time series blended from Landsat and MODIS data for grassland biomass estimation, Remote Sensing, 8, 10, doi:10.3390/rs8010010, 2016.4

Zhang, H., Sun, Y., Chang, L., Qin, Y., Chen, J., Qin, Y., Du, J., Yi, S., and Wang, Y.: Estimation of grassland canopy height and aboveground biomass at the quadrat scale using unmanned aerial vehicle, Remote sensing, 10, 851, doi:10.3390/rs10060851, 2018.4

Zhang, H. F., Tang, Z. G., Wang, B. Y., Meng, B. P., Qin, Y., Sun, Y., Lv, Y. Y., Zhang, J. G., and Yi, S. H.: A non-destructive method for rapid acquisition of grassland aboveground biomass for satellite ground verification using UAV RGB images, Global Ecology and Conservation, 33, e01999, doi:10.1016/j.gecco.2022.e01999, 2022a.4

ZHANG, X., LI, M., WU, J., HE, Y., and NIU, B.: Alpine Grassland Aboveground Biomass and Theoretical Livestock Carrying Capacity on the Tibetan Plateau, Journal of Resources and Ecology, 13, 129-141, 2022b.4

Zhang, Y., Bingyu, L. I., and Zheng, D.: Datasets of the boundary and area of the Tibetan Plateau, ACTA GEOGRAPHICA SINICA, 69, 164-168, 2014.4

Zhang, Y. Q., Tang, Y. H., and Jiang, J. A.: Characterizing the dynamics of soil organic carbon in grasslands on the Qinghai-Tibetan Plateau, 2007.4

Zheng, D.: Natural region system research of Tibetan Plateau, Science in China (Series D), 26, 336–334, 1996.4